Modelling of Non-Equilibrium Electrical Discharges: Streamers and Determination of Electric Field from Optical Emissions

Habilitation thesis

Zdeněk Bonaventura

Masaryk University, Faculty of Science
Department of Plasma Physics and Technology

Brno, January 2026

Contents

1 Modelling of Streamers **9**
1.1 Fluid streamer models 10
1.2 Poisson's equation via Finite Volume Method 12
1.3 Surface processes 16
1.4 Photoionization models 18
1.4.1 Photoionization model in air 18
1.4.2 Photoionization models in N_2,O_2,CO_2 and He 20
1.4.3 Photoionization models for helium plasma jets 21
1.4.4 Kinetic photoionization models 21
1.4.5 Approximate methods for radiative transfer equation 21
1.5 Numerical challenges of fluid streamer modelling 25
1.6 Runaway electrons 28

2 Models for electric field determination from optical emissions in streamers **33**
2.1 Generic Formulation of the Ratio Method 33
2.2 Influence of streamer geometry and light-detection scenarios 34
2.3 Sensitivity analysis and uncertainty quantification of dominant processes for the FNS/SPS ratio method. 36

Abstract

This habilitation thesis is a collection of ten peer-reviewed papers focused on modelling aspects of the propagation of fast ionizing waves known as streamers. Chapter 1 presents key building blocks for a fluid description of streamers: charged-species transport equations; the Poisson equation and its solution using finite-volume methods; an overview of the basic processes required for describing streamer interactions with surfaces; and several computational models used for simulating photoionization in streamers. Numerical challenges associated with streamer modelling are also addressed. Chapter 1 further elaborates on the physics of runaway electrons, including investigations of thermal runaway in streamers and the definition of the runaway threshold.

Chapter 2 focuses on theoretical aspects of electric-field determination from streamer optical emissions using the established and widely used intensity-ratio method. We analyse the effects of different light-detection scenarios in terms of time- and space-integrated recordings. Moreover, a sensitivity analysis and uncertainty quantification of reaction-kinetic datasets were performed in order to provide confidence bands for the ratio method.

List of commented publications

The following list of selected publications is split into two topics. Within each of the topics, the publications are sorted by publication date. My estimated contribution to these publications is specified in the respective tables according to: *work contribution*, *supervision of students*, *manuscript preparation*, and *research direction*.

Topic A contains three selected works which are relevant for theoretical foundations of the electric-field determination in non-thermal transient discharges from optical emission spectroscopy, particularly through the method of intensity ratios. The publication A1 examines the influence of streamer geometry and various light-detection scenarios on the inferred electric fields. Works A2 and A3 aim to derive the ratio methods from detailed non-equilibrium kinetics, and analyze the underlying uncertainties.

Topic B contains seven selected publications and addresses various aspects of streamer physics through numerical modelling. Papers B1–B3 arise from my collaboration with applied mathematicians on developing and applying advanced numerical methods with space–time adaptivity and *a-priori* error control to the modelling of streamer discharges in air. Publications B4–B5 emerged from our interest in the physics of runaway electrons. Publication B6 is a Topical Review on streamer breakdown, where my contribution mainly involves elaboration of Section 4: *Streamer-cathode interaction as a bottleneck in computer simulations of the streamer breakdown*. Publication B7 focuses on approximate methods for numerical solution of radiative transport equation for evaluation of photoionization term in streamer models in air. Note that selected parts of publications B6 and B7 serve as a ground for Chapter 1 of this habilitation thesis.

(A1) **Zdeněk Bonaventura**, Anne Bourdon, Sebastien Celestin, and Victor P Pasko. Electric field determination in streamer discharges in air at atmospheric pressure. *Plasma Sources Science and Technology*, 20(3):035012, 2011. doi: 10.1088/0963-0252/20/3/035012.

Work contribution	Supervision	Manuscript	Research direction
50%	n/a	80%	80%

(A2) Adam Obrusník, Petr Bílek, Tomáš Hoder, Milan Šimek, and **Zdeněk Bonaventura**. Electric field determination in air plasmas from intensity ratio of nitrogen spectral bands: I. Sensitivity analysis and uncertainty quantification of dominant processes. *Plasma Sources Science and Technology*, 27(8):085013, 2018. doi: 10.1088/1361-6595/aad663.

Work contribution	Supervision	Manuscript	Research direction
10%	80%	10%	90%

(A3) Petr Bílek, Adam Obrusník, Tomáš Hoder, Milan Šimek, and **Zdeněk Bonaventura**. Electric field determination in air plasmas from intensity ratio of nitrogen spectral bands: II. Reduction of the uncertainty and state-of-the-art model. *Plasma Sources Science and Technology*, 27(8):085012, 2018. doi: 10.1088/1361-6595/aad666.

Work contribution	Supervision	Manuscript	Research direction
10%	80%	10%	90%

(B1) Max Duarte, **Zdeněk Bonaventura**, Marc Massot, Anne Bourdon, Stéphane Descombes, and Thierry Dumont. A new numerical strategy with space-time adaptivity and error control for multi-scale streamer discharge simulations. *Journal of Computational Physics*, 231(3):1002–1019, 2012. doi: 10.1016/j.jcp.2011.07.002.

Work contribution	Supervision	Manuscript	Research direction
30%	10%	30%	20%

(B2) **Zdeněk Bonaventura**, Max Duarte, Anne Bourdon, and Marc Massot. Derivation of a merging condition for two interacting streamers in air. *Plasma Sources Science and Technology*, 21(5):052001, 2012. doi: 10.1088/0963-0252/21/5/052001.

Work contribution	Supervision	Manuscript	Research direction
60%	n/a	80%	60%

(B3) Max Duarte, **Zdeněk Bonaventura**, Marc Massot, and Anne Bourdon. A numerical strategy to discretize and solve the poisson equation on dynamically adapted multiresolution grids for time-dependent streamer discharge simulations. *Journal of Computational Physics*, 289:129–148, 2015. doi: 10.1016/j.jcp.2015.02.038.

Work contribution	Supervision	Manuscript	Research direction
30%	n/a	30%	20%

(B4) Olivier Chanrion, **Zdeněk Bonaventura**, Deniz Çinar, Anne Bourdon, and Torsten Neubert. Runaway electrons from a 'beam-bulk' model of streamer: application to TGFs. *Environmental Research Letters*, 9(5):055003, 2014. doi: 10.1088/1748-9326/9/5/055003.

Work contribution	Supervision	Manuscript	Research direction
35%	n/a	20%	20%

(B5) Olivier Chanrion, **Zdeněk Bonaventura**, Anne Bourdon, and Torsten Neubert. Influence of the angular scattering of electrons on the runaway threshold in air. *Plasma Physics and Controlled Fusion*, 58(4):044001, 2016. doi: 10.1088/0741-3335/58/4/044001.

Work contribution	Supervision	Manuscript	Research direction
35%	n/a	20%	20%

(B6) Mirko Černák, Tomáš Hoder, and **Zdeněk Bonaventura**. Streamer breakdown: cathode spot formation, Trichel pulses and cathode-sheath instabilities. *Plasma Sources Science and Technology*, 29(1):013001, 2019. doi: 10.1088/1361-6595/ab5051.

Work contribution	Supervision	Manuscript	Research direction
15%	n/a	15%	5%

(B7) Jan Tungli, Miroslav Horký, Stanislav Kadlec, and **Zdeněk Bonaventura**. Capturing photoionization shadows in streamer simulations using the discrete ordinates method. *Plasma Sources Science and Technology*, 32(10):105009, 2023. doi: 10.1088/1361-6595/acfcd8.

Work contribution	Supervision	Manuscript	Research direction
10%	80%	20%	50%

Preface

The beginning of my post-phd life dates back to 2007, where I attended one month post-doc stay at Laboratoire SIAME, UFR Sciences, Université de Pau et des Pays de l'Adour in south of France. My task there was to develop a procedure for a solution of Poisson's equation using a finite volume method, which would allow for consideration of charge distributions on dielectric surfaces. This proved to be the decisive and door opening moment for my future path, as my journey then led to Laboratoire EM2C at Ecole Centrale Paris in February 2008, where I acquired a six-month post-doc under advisory of prof. Anne Bourdon (our collaboration is still ongoing to this very day). My work there at EM2C was to participate in development of streamer simulation code. Thanks to my natural inclination towards technical aspects of the problems, I gravitated to work on performance enhancements of the steamer code, particularly in terms of shared memory parallelization based on OpenMP. This actually turned out to be rather straightforward, yet game-changing enhancement of the streamer code, allowing us to shorten the computational time from the initial three weeks per single run, to more reasonable run time of couple of days. Another parallel line of attack to gain enhanced performance in the streamer code, was via employment of then-emerging-to-prominence direct sparse solvers, where SuperLU, MUMPS and AGMG are honorable mentions. This required to master cross-language interoperability, and my realisation that the underscore '_' may be there, even if it is not.

Later, this path evolved into collaboration with applied mathematicians Dr. Max Duarte and Prof. Marc Massot, aiming at development and implementation of adaptive numerical methods for evolutionary partial differencial quations, both in space and time, allowing for a-priori error control. Space adaptivity was provided by means of multiresolution analysis, which back then reqiured not only thinking a lot in recursive manner, but also learing to grow trees upside-down.

Next in the line of my professional path was an intense venture to the physics of runaway electrons via collaboration with Dr. Olivier Chanrion from DTU Space in Denmark. The idea was to merge the fluid model for streamer propagation and the Particle-In-Cell model for streamers developed by Olivier Chanrion. At that time, Anne Bourdon moved from EM2C to LPP (Laboratoire de physique des plasmas, Ecole Polytechnique) and so my regular reseach visites. The interest was to study the thermal runaway process in which the 'low energy electrons' are accelerated to 'high energies' in front of the negative streamers, where the electric field is strongly enhanced. Standard (and over simplified) picture says that these electrons would accelerate in the applied electric field indefinitely, because the friction force acting on them via inelastic collisions with air molecules decreases with increasing electron energy. We ended up revisiting this runaway threshold by introducing the effects of angular scattering of electrons.

My path in streamer simulations also bloomed to fruitful collaboration with Dr. Milan Šimek (Institute of Plasma Physics (IPP), Czech Academy of Science), who is a world

leading expert in cutting edge spectroscopy methods and streamer diagnostics. With Milan, we were fortunate to obtain a Czech Science Foundation project, which allowed us to join forces and focus on air streamer kinetics, from experimental as well as theoretical point of view. Consequently, we also obtained another Czech Science Foundation projects, focusing on fast pulsed nanosecond breakdown of liquid water, and resulting in broad and exciting scientific investigations [1–4]. Last but not least, with the IPP team, another Czech Science Foundation project starts in January 2026, where we aim to study the interaction of transient sparks with water surface.

This habilitation thesis is based on research papers which I authored or co-authored. Some parts of these papers were adapted for this thesis to provide basic self-consistent overview of the topics covered. For the two chapters, the corresponding principal references are: (1) Modelling of Streamers [5–12], (2) Models for electric field determination from optical emission in streamer discharges [13–17].

Chapter 1

Modelling of Streamers

Streamer breakdown theory, introduced more than 80 years ago through the works of Reather [18] and Loeb and Meek [19], was formulated to explain the rapid breakdown observed in spark discharges within overvolted gaps at atmospheric pressure. This theory emerged from the understanding that the short duration of this swift breakdown was insufficient for ions to traverse the gap between the electrodes—a key premise of the classical Townsend theory which was grounded in secondary emission processes [20]. Newly emerging breakdown theory was based on a concept of a *streamer*. Streamer is a contracted *ionizing wave* with self-generated electric field enhancement that propagates into a low-ionized medium exposed to high electric field, leaving a filamentary trails of plasma behind [21–24]. Typical structure of the discharge event created by propagating streamer front is depicted in Figure 1.1, showing high electron density within the discharge filament, and the enhanced electric field at the discharge front. A crucial parameter that describes a streamer is its peak electric field. This field represents a primary objective of many experimental investigations and holds eminent interest in simulations of streamer plasmas [13, 25–40]. The peak electric field is associated with the net space charge in a region called a 'streamer head', and in air typically attains values between 4 and 7 times of the conventional breakdown threshold, which is $E_{\mathrm{cbt}} \sim 3\,\mathrm{MV/m}$ at standard temperature and pressure. The high electric field in the streamer head leads to intense electron impact ionization: the essential physical process which drives the streamer propagation. Streamers can propagate at astonishing speeds,

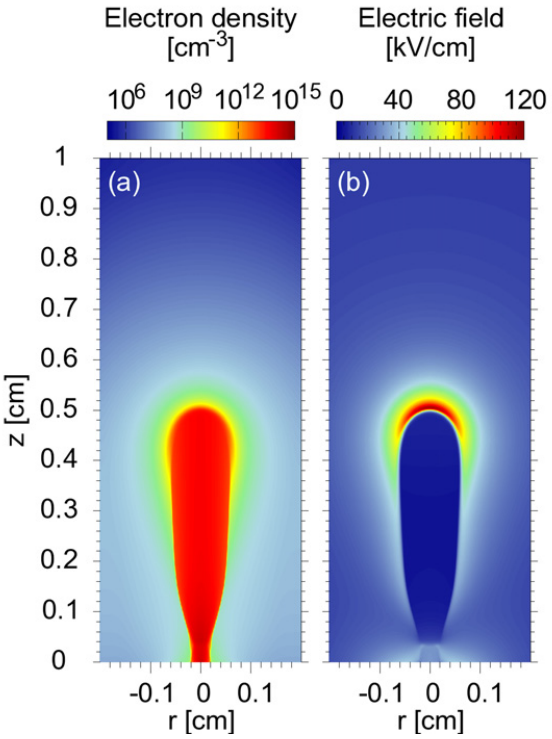

Figure 1.1: Cross sectional views of electron density (a), electric field (b), respectively, for a positive streamer. Figure reprinted from [13].

sometimes reaching up to 1% of the speed of light. At atmospheric pressure, a typical streamer-generated plasma filament has a radius of approximately 10^{-3} m.

Another important characteristic of streamers is their *polarity*. The polarity of a streamer is determined by the sign of the space charge in its head, leading to their classifications as being either positive or negative. Positive streamers propagate against the direction of the electron drift and require ambient seed charges for continued propagation, see figure 1.2. In contrast, the negative streamer can propagate without seed electrons because electron avalanches originate from the streamer head and move in the same direction as the streamer. Streamers serve as precursors to various discharge phenomena, including sparks, lightning leaders, and high-altitude discharges such as sprites and blue jets [42]. In gas mediums, streamer discharges generate charged species and, in laboratory settings, can also do so on surfaces. They initiate distinct chemical reactions due to the excited atomic and molecular states they create [43–50]. Moreover, streamers can induce gas flow through electrohydrodynamic forces [51]. These phenomena have paved the way for a myriad of technological applications. For a more comprehensive list of references on these topics, the reader is referred to [21, 37, 52, 53].

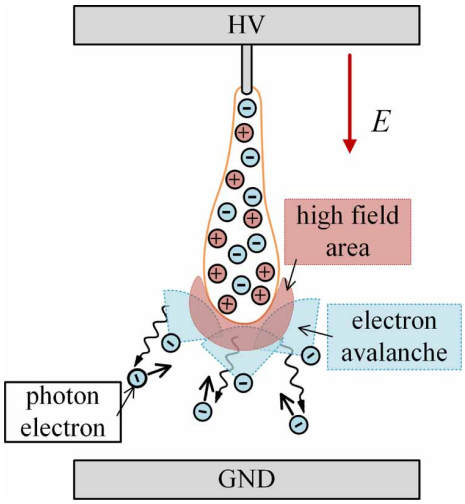

Figure 1.2: Schematic illustration of self-sustained positive streamer propagation due to seed electrons produced by photoionization process. The streamer grows due to incoming electron avalanches. Seed electrons for the electron avalanches may be generated by photoionizing radiation originating from the streamer itself or from preionisation caused by other sources. Figure reprinted from [41].

1.1 Fluid streamer models

The propagation of streamers can be modelled using a truncated set of moments of the Boltzmann equation for charged species. This approximation gives a set of fluid equations which need to be coupled with Poisson's equation for electric potential in order to account for mutual interaction of charged particles through the electric forces. This truncated set of moments comprises the continuity equation and the momentum equations. The continuity equations for the density n_α, for charged species of type α, are given by:

$$\frac{\partial n_\alpha}{\partial t} + \boldsymbol{\nabla} \cdot \boldsymbol{\Gamma}_\alpha = G_\alpha - L_\alpha, \tag{1.1}$$

where G_α and L_α denote production and loss terms, respectively, and $\boldsymbol{\Gamma}_\alpha$ represents the flux of density n_α due to the macroscopic motion of the fluid. Typically, at atmospheric pressure, the momentum equations can be effectively approximated using so called *drift-diffusion approximation*. In this approach, fluid momentum is assumed to be in local equilibrium: the driving forces, whether arising from the electric field (drift) or from gradients in density (diffusion), are counterbalanced by the frictional effects of collisions. This ensures that the net acceleration of the fluid remains zero. This approximation holds true when the mean free path of particles is considerably smaller than the characteristic

spatial scale of variation of physical quantities, such as n_α and the electric field $\mathbf{E}$. Note that the mean free path for electrons at atmospheric pressure is approximately 10^{-7} m, whereas the spatial scale of variation of the electric field in the head of the ionization wave is around 10^{-5} m. Given that both, the drift and the diffusion components in the momentum equations are balanced by collisions, the fluid flux $\mathbf{\Gamma}_\alpha$ under the drift-diffusion approximation is:

$$\mathbf{\Gamma}_\alpha = \frac{q_\alpha}{|q_\alpha|} n_\alpha \mu_\alpha \mathbf{E} - D_\alpha \boldsymbol{\nabla} n_\alpha. \tag{1.2}$$

In this equation n_α, μ_α, D_α and q_α denote the density, mobility, diffusion coefficient, and charge of a specie α, respectively.

Furthermore, it is often also assumed that the energy gained by electrons from the electric field is locally counteracted due to collisions with neutrals. Note that the collision frequency of electrons with neutrals at atmospheric pressure is in the order of $\nu_{\text{en}} = 10^{13}$ Hz. As such, the electron energy distribution function relaxes to the equilibrium with the local electric field on a timescale of ν_{en}^{-1}. Consequently, the need to solve the electron energy equation is bypassed by referencing the mean electron energy from a precomputed solution of the stationary electron Boltzmann equation for the corresponding electric field. This approach, known as the *local-field approximation*, is particularly well-justified for describing electrons in streamers that propagate in volume, as evidenced by comparisons to Particle In Cell / Monte Carlo (PIC/MCC) simulations in [54]. The transport parameters, i.e. μ_α and D_α, in (1.2) and reaction rates in the gain and loss terms of (1.1) then become functions of the reduced electric field $|\mathbf{E}|/N_{\text{gas}}$, see figure 1.3.

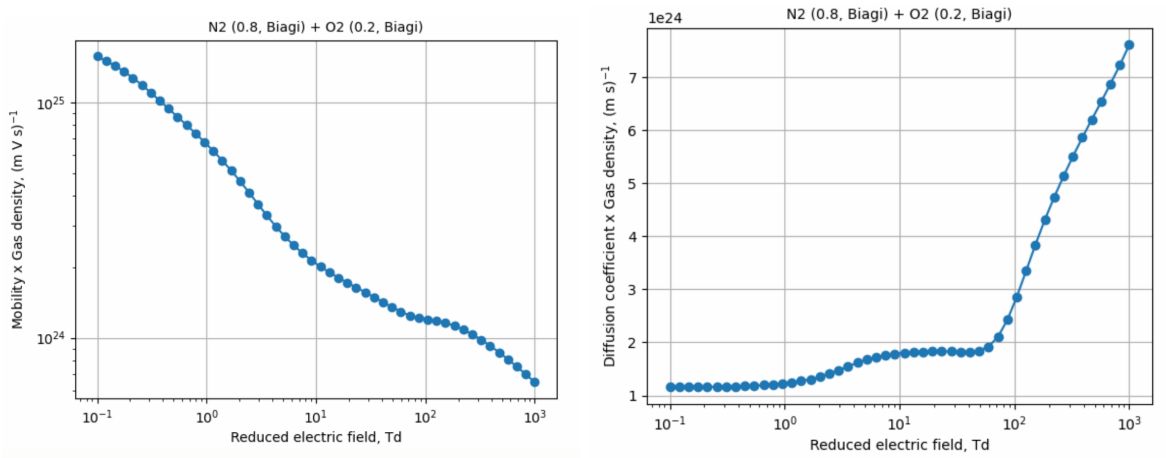

Figure 1.3: Reduced mobility and diffusion coefficient for N2/O2 (0.8/0.2) gas mixture. Source: BOLSIG+ solver ver. 03/2016, `www.lxcat.net`, Biagi database (N2,O2), retrieved on December 16, 2025.

There are situations where the local field approximation is insufficient, for example in discharge regions where strong spatial variations of the electric field are present, such as in sheath regions close to electrodes, as we highlighted in our work

(B6) Mirko Černák, Tomáš Hoder, and **Zdeněk Bonaventura**. Streamer breakdown: cathode spot formation, Trichel pulses and cathode-sheath instabilities. *Plasma Sources Science and Technology*, 29(1):013001, 2019. doi: 10.1088/1361-6595/ab5051.

In these situations, incorporating energy transport for electrons is beneficial. The resulting approximation is referred to as the *local mean energy approximation*. The electron energy equation can be derived from the electron Boltzmann equation [55] and can be transformed to acquire a form similar to (1.1):

$$\frac{\partial n_\varepsilon}{\partial t} + \boldsymbol{\nabla} \cdot \boldsymbol{\Gamma}_\varepsilon + e_0 \boldsymbol{\Gamma}_\mathrm{e} \cdot \mathbf{E} = G_\varepsilon - L_\varepsilon. \tag{1.3}$$

Here n_ε denotes the energy density, and e_0 is the elementary charge. Term $\boldsymbol{\Gamma}_\mathrm{e} \cdot \mathbf{E}$ accounts for electron heating by the electric field, while the right-hand side encapsulates the total energy gains and losses resulting from collisions. The energy flux $\boldsymbol{\Gamma}_\varepsilon$ can also be formulated in a drift-diffusion manner [55]:

$$\boldsymbol{\Gamma}_\varepsilon = n_\varepsilon \mu_\varepsilon \mathbf{E} - D_\varepsilon \boldsymbol{\nabla} n_\varepsilon, \tag{1.4}$$

where μ_ε and D_ε denotes the energy mobility and the energy diffusion coefficient, respectively. This formulation of the electron energy equation is advantageous because the energy density can be treated simply as an additional species. Electron transport parameters and reaction rates for electron-impact processes can also be readily derived from the relevant cross-section sets using BOLSIG+ [55], or the LXCat project `https://lxcat.net/`, see also [56–58].

The transport equations (1.1)–(1.4) must be solved together with Poisson's equation

$$\boldsymbol{\nabla} \cdot (\varepsilon_0 \varepsilon_\mathrm{r} \boldsymbol{\nabla} \phi) = -\sum_\alpha q_\alpha n_\alpha - \delta_\mathrm{s} \sigma_\mathrm{s}, \qquad \mathbf{E} = -\boldsymbol{\nabla} \phi, \tag{1.5}$$

where ϕ represents the electric potential, ε_0 and ε_r represent the permittivity of free space and relative permittivity of materials, e.g. dielectrics. Then the term $\delta_\mathrm{s}\sigma_\mathrm{s}$ accounts for surface charge densities on the dielectric surfaces.

It's important to note that Poisson's equation operates under the electrostatic approximation, which implies the absence of magnetic fields originating from internal currents flowing in the plasma. In the streamer scenario, magnetic forces on charged particles due to internal currents are negligible compared to the electric forces. An illustrative calculation can be performed to compare the relative magnitudes of electric and magnetic forces for a 'typical' streamer. Consider a streamer channel with an electric current density generated by electrons drifting under the influence of the electric field. Using Ampere's law to determine the magnetic field, and assuming typical conditions for air streamers: atmospheric pressure air density $N_\mathrm{gas} = 2.7 \times 10^{25}\ \mathrm{m}^{-3}$, streamer radius $R_s = 1$ mm, electron density $n_e = 10^{19}\ \mathrm{m}^{-3}$, reduced electric field E/N_gas of 200 Td ($1\,\mathrm{Td} = 10^{-21}\mathrm{V}\cdot\mathrm{m}^2$) and scaled electron mobility $\mu_e N_\mathrm{gas} \approx 10^{24}\ \mathrm{m}^{-1}\mathrm{V}^{-1}\mathrm{s}^{-1}$, the estimated ratio of the magnetic force to the electric force is given by:

$$f_B/f_E = \frac{\mu_0}{2} e_0 n_e \mu_e^2 E R_\mathrm{s} = \frac{\mu_0 e_0 n_e}{2 N_\mathrm{gas}} (\mu_e N_\mathrm{gas})^2 \, (E/N_\mathrm{gas}) \, R_\mathrm{s} \approx 10^{-5}.$$

Therefore the magnetic forces from internal currents in the context of streamer dynamics can be neglected.

1.2 Poisson's equation via Finite Volume Method

An efficient and accurate solution of Poisson's equation is crucial for modelling streamer discharges because the electric field-obtained as the gradient of the electrostatic potential

directly governs the streamer's ionization dynamics. Even small numerical errors in the potential can lead to large local errors in the electric field, which in turn strongly affect electron impact ionization rates, space-charge formation, and the stability of ionization fronts. In this section we introduce Finite Volume Method (FMV) to discretize the Poisson's equation. The FVM is a numerical technique for solving partial differential equations that come from conservation laws, such as mass, momentum, charge, or energy conservation. Instead of approximating the equations at points, FVM divides the domain into small control volumes, or cells, see figure 1.4, and enforces that the net flux of the conserved quantity across the boundary of each volume balances the sources inside it. This guarantees local conservation by construction.

Let us consider the Poisson's equation for the electric potential $\phi(x)$ in the form

$$-\nabla \cdot (\varepsilon(\mathbf{x})\nabla\phi(\mathbf{x})) = \rho(\mathbf{x}), \tag{1.6}$$

where $\varepsilon(\mathbf{x})$ is a discontinuous function of a position $\mathbf{x}$ and $\rho(\mathbf{x})$ is the electric charge density.[1] In order to find the FVM representation of equation (1.6) we consider its integral form over a selected control volume Ω_i:

$$-\int_{\Omega_i} \nabla \cdot (\varepsilon(\mathbf{x})\nabla\phi(\mathbf{x}))\ \mathrm{d}V = \int_{\Omega_i} \rho(\mathbf{x})\,\mathrm{d}V.$$

Applying the divergence theorem we obtain

$$-\int_{\partial\Omega_i} (\varepsilon(\mathbf{x})\nabla\phi(\mathbf{x})) \cdot \hat{\mathbf{n}}\,\mathrm{d}S = \int_{\Omega_i} \rho(\mathbf{x})\,\mathrm{d}V, \tag{1.7}$$

where $\hat{\mathbf{n}}$ is the unit normal vector—pointing outward from Ω_i—defined for the boundary $\partial\Omega_i$ of the control volume.

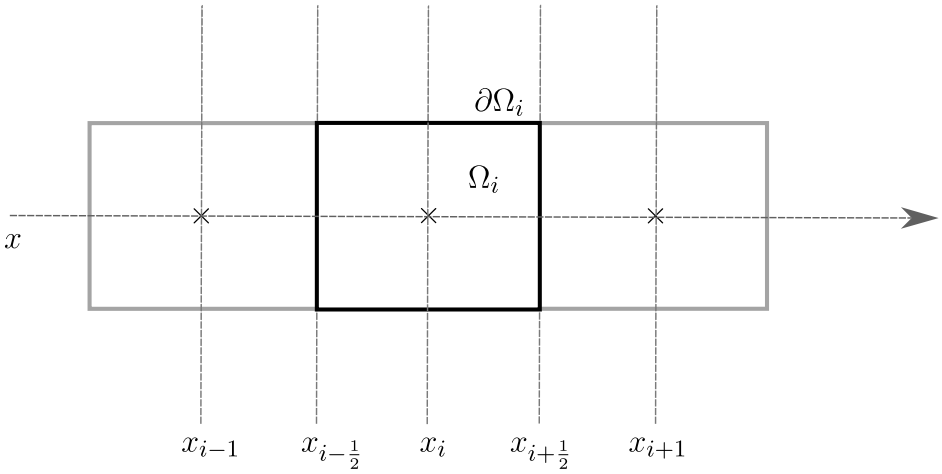

Figure 1.4: Discretization of space into control volumes. Control volume Ω_i is centered at x_i, its left interface is located at $x_{i-\frac{1}{2}}$, and its right interface is located at $x_{i+\frac{1}{2}}$.

For illustration, let us show the derivation of the FVM representation of (1.7) in one dimension, the procedure can be readily generalized in more dimensions. The left hand

[1]The discontinuity in the dielectric function allows us to solve Poisson's equation in presence of dielectrics, the derived discrete equations will also be generalized to take into account surface charges on dielectric surfaces. It is particularly relevant for simulating interaction of streamers with dielectric barriers, or in plasma jets, as we did for example in our works [6, 59].

side of (1.7) reads

$$-\int_{\partial\Omega_i}\left(\varepsilon(x)\frac{\partial\phi(x)}{\partial x}\right)\cdot\hat{\mathbf{n}}\,\mathrm{d}S=\int_L\left(\varepsilon(x)\frac{\partial\phi(x)}{\partial x}\right)\,\mathrm{d}S-\int_R\left(\varepsilon(x)\frac{\partial\phi(x)}{\partial x}\right)\,\mathrm{d}S,$$

where the outer normal $\hat{\mathbf{n}}$ points towards decreasing x at the left (L) interface, but towards increasing x for the right (R) interface of the control volume $\partial\Omega_i$, defining thus the sign of the integral contributions.

Ordinary cell

For an ordinary cell Ω_i, with no jump in the value of ε within the cell or on its edges, nor at the neighbouring cells, we can use central difference approximation for the derivatives of $\phi(x)$

$$\left.\frac{\partial\phi(x)}{\partial x}\right|_L\approx\frac{\phi_i-\phi_{i-1}}{x_i-x_{i-1}},\qquad\left.\frac{\partial\phi(x)}{\partial x}\right|_R\approx\frac{\phi_{i+1}-\phi_i}{x_{i+1}-x_i},$$

where $\phi_i=\phi(x_i)$ and $\phi_{i\pm1}=\phi(x_{i\pm1})$. We obtain a descrete equation which has a tridiagonal form

$$(R_i+L_i)\phi_i-R_i\phi_{i+1}-L_i\phi_{i-1}=\rho_i,$$

with

$$R_i=\frac{\varepsilon}{(x_{i+1}-x_i)(x_{i+\frac{1}{2}}-x_{i-\frac{1}{2}})},\qquad L_i=\frac{\varepsilon}{(x_i-x_{i-1})(x_{i+\frac{1}{2}}-x_{i-\frac{1}{2}})},$$

and $\rho_i=\rho(x_i)$ representing the charge density in a cell Ω_i. Note also that the term $(x_{i+1/2}-x_{i-1/2})$ is, in fact, a width of the cell from the integration of the right hand side of (1.7) over the volume of Ω_i, see figure 1.4.

Cell with a permittivity jump on its edge

Assume a jump of permittivity at $x_{i+1/2}$ as shown in figure 1.5. The existence of the

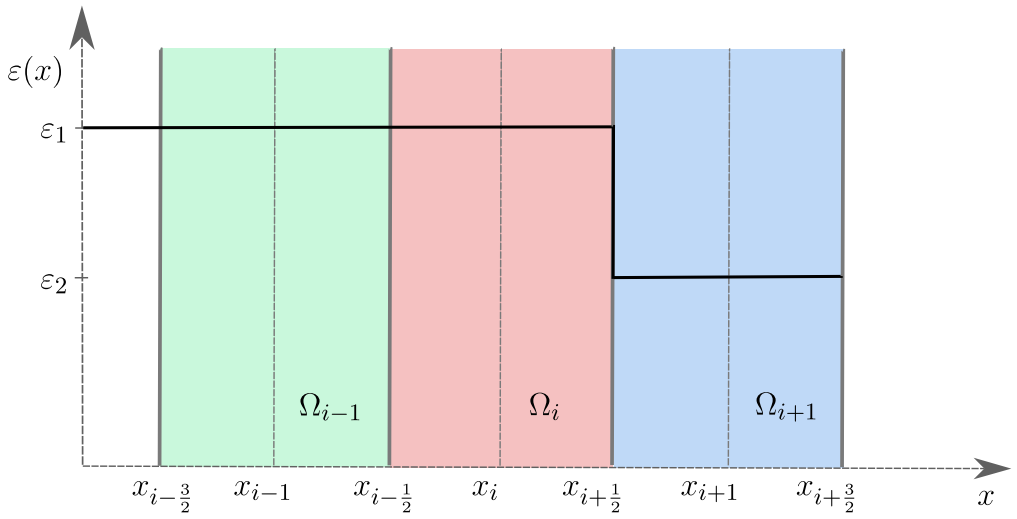

Figure 1.5: Permittivity jump at $x_{i+\frac{1}{2}}$.

jump in ε will have an influence

- on the discrete equation for cell Ω_i,

- as well as on the discrete equation for cell Ω_{i+1}.

The jump condition for the normal component of the electric field on the interface between two dielectrics of permittivity ε_1 (on the left from the interface) and ε_2 (on the right from the interface) is

$$\varepsilon_1 E_1 = \varepsilon_2 E_2, \tag{1.8}$$

where E_1 corresponds to the electric field on the left from the interface, while E_2 corresponds to the electric field on the right from the interface.

Discrete form of this jump condition using forward and backward differences is

$$\varepsilon_1 \frac{\phi_{i+\frac{1}{2}} - \phi_i}{x_{i+\frac{1}{2}} - x_i} = \varepsilon_2 \frac{\phi_{i+1} - \phi_{i+\frac{1}{2}}}{x_{i+1} - x_{i+\frac{1}{2}}}.$$

From there we obtain

$$\phi_{i+\frac{1}{2}} = \frac{\varepsilon_2(x_{i+\frac{1}{2}} - x_i)}{\varepsilon_1(x_{i+1} - x_{i+\frac{1}{2}}) + \varepsilon_2(x_{i+\frac{1}{2}} - x_i)}\phi_{i+1} + \frac{\varepsilon_1(x_{i+1} - x_{i+\frac{1}{2}})}{\varepsilon_1(x_{i+1} - x_{i+\frac{1}{2}}) + \varepsilon_2(x_{i+\frac{1}{2}} - x_i)}\phi_i. \tag{1.9}$$

Using forward and backward differences we can also obtain discrete approximations of finite volume equation (1.7) for the i-th cell:

$$\varepsilon_1 \frac{\phi_i - \phi_{i-1}}{(x_i - x_{i-1})(x_{i+\frac{1}{2}} - x_{i-\frac{1}{2}})} - \varepsilon_1 \frac{\phi_{i+\frac{1}{2}} - \phi_i}{(x_{i+\frac{1}{2}} - x_i)(x_{i+\frac{1}{2}} - x_{i-\frac{1}{2}})} = \rho_i, \tag{1.10}$$

and for the $(i+1)$-th cell

$$\varepsilon_2 \frac{\phi_{i+1} - \phi_{i+\frac{1}{2}}}{(x_{i+1} - x_{i+\frac{1}{2}})(x_{i+\frac{3}{2}} - x_{i+\frac{1}{2}})} - \varepsilon_2 \frac{\phi_{i+2} - \phi_{i+1}}{(x_{i+2} - x_{i+1})(x_{i+\frac{3}{2}} - x_{i+\frac{1}{2}})} = \rho_{i+1}. \tag{1.11}$$

In order to conserve the tridiagonal shape of the resulting matrix, we have to replace $\phi_{i+\frac{1}{2}}$ in equations (1.10) and (1.11) by (1.9). After some rearrangements, this procedure leads to the final discrete equations for i-th cell (the cell right on the left of the interface) in the desired form

$$-R_L\phi_{i+1} - L_L\phi_{i-1} + (R_L + L_L)\phi_i = \rho_i, \tag{1.12}$$

where

$$R_L = \frac{\varepsilon_1\varepsilon_2}{\left(\varepsilon_1(x_{i+1} - x_{i+\frac{1}{2}}) + \varepsilon_2(x_{i+\frac{1}{2}} - x_i)\right)(x_{i+\frac{1}{2}} - x_{i-\frac{1}{2}})},$$

$$L_L = \frac{\varepsilon_1}{(x_i - x_{i-1})(x_{i+\frac{1}{2}} - x_{i-\frac{1}{2}})}.$$

For the $(i+1)$-th cell the discrete equation has the same form as well:

$$-R_R\phi_{i+2} - L_R\phi_i + (R_R + L_R)\phi_{i+1} = \rho_{i+1}, \tag{1.13}$$

where

$$R_R = \frac{\varepsilon_2}{(x_{i+2} - x_{i+1})(x_{i+\frac{3}{2}} - x_{i+\frac{1}{2}})},$$

$$L_R = \frac{\varepsilon_1\varepsilon_2}{\left(\varepsilon_1(x_{i+1} - x_{i+\frac{1}{2}}) + \varepsilon_2(x_{i+\frac{1}{2}} - x_i)\right)(x_{i+\frac{3}{2}} - x_{i+\frac{1}{2}})}.$$

Introduction of surface charge

In cases where non-zero surface charge of density $\sigma_{i+\frac{1}{2}}$ at $x_{i+\frac{1}{2}}$ is present, the jump condition (1.8) is changed to $-\varepsilon_1 E_1 + \varepsilon_2 E_2 = \sigma$. Resolution for $\phi_{i+\frac{1}{2}}$ now gives

$$\begin{aligned}\phi_{i+\frac{1}{2}} = &\frac{\varepsilon_2(x_{i+\frac{1}{2}} - x_i)}{\varepsilon_1(x_{i+1} - x_{i+\frac{1}{2}}) + \varepsilon_2(x_{i+\frac{1}{2}} - x_i)}\phi_{i+1} \\ &+ \frac{\varepsilon_1(x_{i+1} - x_{i+\frac{1}{2}})}{\varepsilon_1(x_{i+1} - x_{i+\frac{1}{2}}) + \varepsilon_2(x_{i+\frac{1}{2}} - x_i)}\phi_i \\ &+ \frac{(x_{i+\frac{1}{2}} - x_i)(x_{i+1} - x_{i+\frac{1}{2}})}{\varepsilon_1(x_{i+1} - x_{i+\frac{1}{2}}) + \varepsilon_2(x_{i+\frac{1}{2}} - x_i)}\sigma_{i+\frac{1}{2}},\end{aligned} \tag{1.14}$$

which is the same as (1.9) but with the last term added. Even if the surface charges are present, the equations (1.12) and (1.13) will have the same form, but on the right hand side there will appear an additional source term taking into account the $\sigma_{i+\frac{1}{2}}$. For the i-th cell the total source term will be

$$i\text{-th cell:} \quad \rho_i + \frac{(x_{i+1} - x_{i+\frac{1}{2}})\varepsilon_1\sigma_{i+\frac{1}{2}}}{(x_{i+\frac{1}{2}} - x_{i-\frac{1}{2}})\left[\varepsilon_1(x_{i+1} - x_{i+\frac{1}{2}}) + \varepsilon_2(x_{i+\frac{1}{2}} - x_i)\right]}. \tag{1.15}$$

For the $(i+1)$-th cell the total source term will be

$$(i+1)\text{-th cell:} \quad \rho_{i+1} + \frac{(x_{i+\frac{1}{2}} - x_i)\varepsilon_2\sigma_{i+\frac{1}{2}}}{(x_{i+\frac{3}{2}} - x_{i+\frac{1}{2}})\left[\varepsilon_1(x_{i+1} - x_{i+\frac{1}{2}}) + \varepsilon_2(x_{i+\frac{1}{2}} - x_i)\right]}. \tag{1.16}$$

To conclude, the 1D finite-volume discretization of Poisson's equation presented above provides a consistent and conservative framework in which the electrostatic potential is expressed directly in terms of fluxes across control-volume interfaces. The derivation highlights how the finite-volume formulation may also naturally incorporate charged dielectric surfaces, while still yielding a symmetric, well-posed linear system suitable for efficient numerical solution. These properties form the basis for extending the method to higher dimensions and to adaptively refined meshes, as for example in our work [11], where the same flux-based formulation ensures accuracy and robustness.

1.3 Surface processes

Surface processes relevant for streamer simulations involve several phenomena, e.g. secondary electron emission through ion impact, or photoemission of electrons. Another processes involved are thermionic and field emissions. These we took into account, for instance, in investigations of delays in discharge re-ignition behind dielectric barriers, as detailed in our work [59].

Secondary electron emission

When exposed to ion bombardment, conducting electrode surfaces can emit secondary electrons. The electron flux emitted from these surfaces, represented as $\mathbf{\Gamma}_{\text{se}}$, is generally

considered proportional to the flux of the impinging ions $\mathbf{\Gamma}_i$:

$$\mathbf{\Gamma}_{\mathrm{se}} \cdot \mathbf{n}_{\mathrm{s}} = -\gamma_{\mathrm{se}} \sum_{i \in \mathrm{ions}} \mathbf{\Gamma}_i \cdot \mathbf{n}_{\mathrm{s}}, \tag{1.17}$$

The proportionality factor here is the secondary emission coefficient, γ_{se}, and $\mathbf{n}_{\mathrm{s}}$ is the surface normal vector. It's worth noting that specifying an exact value for γ_{se} is usually not possible; a typical values usually considered range between 0.001 and 0.1. Higher values of γ_{se} may be employed as crude approximation to account for other electron emission processes, including impacts from excited species and field emission. Effective process for generating secondary electrons is through the Auger neutralization [60, 61]. During this process, an electron from the surface tunnels into an approaching ion, effectively neutralizing it. When the energy difference between the ionization potential I of the approaching ion and the work function W of the material exceeds W, this energy can facilitate the ejection of another emission electron. Consequently, the kinetic energy of the emitted electron is described by the energy difference $I - 2W$. As an example can be considered an ionization potential of 12.1 eV coresponding to oxygen, and a typical work function of 4 eV, then the energy of the secondary electrons is thus about 4 eV [61].

Photoemission

Another physical mechanism generating secondary electrons in streamer discharges that are in contact with surfaces is photoemission. The flux of photoelectrons can be expressed by

$$\mathbf{\Gamma}_{\mathrm{pe}} \cdot \mathbf{n}_s = -\gamma_{\mathrm{pe}}\, \boldsymbol{\varphi} \cdot \mathbf{n}_s. \tag{1.18}$$

Here γ_{pe} represents the coefficient for photoemission, and $\boldsymbol{\varphi}$ denotes the photon flux impacting at the surface. The photon flux at an observation point $\mathbf{r}$ due to a source point at $\mathbf{r}'$ can be expressed as:

$$\boldsymbol{\varphi}(\mathbf{r}) = \frac{1}{4\pi} \int_{V'} \frac{I(\mathbf{r}')(\mathbf{r} - \mathbf{r}')}{|\mathbf{r} - \mathbf{r}'|^3} \exp(-\mu |\mathbf{r} - \mathbf{r}'|)\, \mathrm{d}V', \tag{1.19}$$

where $I(\mathbf{r}')$ is the photon production rate and is often equated to the ionization production rate [62, 63]. Additionally, μ characterizes photon absorption, which is frequently assumed negligible [64]. Consequently, γ_{pe} is the sole coefficient required to model the photoemission source term, as we did in our work [65].

The Thermionic Emission Process

The thermionic emission refers to the ejection of electrons from a metallic cathode due to the cathode's thermal energy. The current density j_{te} at the cathode surface, resulting from thermionic emission, can be expressed as follows, see [66]:

$$j_{\mathrm{te}} = \frac{1}{2} \left(\frac{kT}{\pi} \right)^2 \frac{\pi d}{\sin(\pi d)} \cdot \exp\left(-\frac{W - F^{1/2}}{kT} \right). \tag{1.20}$$

It's important to note that this equation is presented in Hartree units. Consequently, the current density j_{te} represents the current per unit area divided by $m_{\mathrm{e}}^3 e^9 \hbar^{-7} \approx 2.36 \times 10^{18}\, A/m^2$, where m_{e} is the electron mass, e is the elementary charge, and $\hbar$ is the reduced Planck's constant. Additionally, $F = (\beta E)/(m_{\mathrm{e}}^2 e^5 \hbar^{-4})$ is proportional to the

electric field strength E, magnified by the amplification factor β, with $m_e^2 e^5 \hbar^{-4} \approx 5.14 \times 10^{11}$V/m. The terms kT and W represent the thermal energy and the work function of the material, respectively. When expressed in eV, they need to be divided by $me^4\hbar^{-2} \approx 27.2\,V$. Furthermore, $d = F^{3/4}(\pi kT)^{-1}$. It is crucial to emphasize that the applicability of equation (1.20) is bounded by $d \leq 1$. It's also noteworthy that when d is sufficiently small, the term $\pi d/\sin(\pi d)$ can be replaced by one, causing the equation (1.20) to simplify to the standard Richardson-Schottky equation. For a more detailed discussion, refer to [66].

The Field Emission Process

The field emission process refers to the ejection of electrons from a metallic cathode due to the presence of a strong electric field, which enhances the tunneling of electrons through the field-deformed surface barrier. The corresponding current density j_f is given by:

$$j_{\mathrm{f}} = \frac{F^2}{16\pi^2 W t^2}\left(\frac{\pi ckT}{\sin(\pi ckT)}\right)\exp\left(\frac{-4\sqrt{2}W^{3/2}v}{3F}\right). \tag{1.21}$$

Again, this expression employs Hartree units, and the meanings of F and W are consistent with those in equation (1.20). Additionally, $c = 2\sqrt{2}F^{-1}W^{1/2}t(F^{1/2}/W)$, where t can be defined by $3t(y) = 4s(y) - v(y)$, with $s(y)$ and $v(y)$ being special functions tabulated in [67] for $y \leq 1$. When ckT is sufficiently small such that the term $\pi ckT/\sin(\pi ckT)$ can be replaced by one, equation (1.21) simplifies to the Fowler–Nordheim formula. The applicability of equation (1.21) is constrained by $ckT < 1$. For a more in-depth discussion, please see [66]. Notably, the field emission process, when combined with positive-ion bombardment at the cathode, was employed in negative streamer simulations. These simulations demonstrated the role of field-effect emission in both the ignition and development of negative coronas, as detailed in [68, 69].

Dielectric Surface charging

Dielectric surfaces can accumulate charge due to the fluxes $\mathbf{j}_\alpha$ of all charged particles of type α with charge q_α. Consequently, the net surface charge density, σ is derived through time integration:

$$\sigma = \sigma_0 - \int_t \sum_\alpha \frac{q_\alpha}{|q_{\mathrm{e}}|}\mathbf{j}_\alpha \cdot \mathbf{n}_{\mathrm{s}}\,\mathrm{d}t,$$

where σ_0 represents the initial charge distribution on the dielectric surfaces, potentially stemming from prior discharge events, and $\mathbf{n}_{\mathrm{s}}$ is the outward normal to the dielectric surface. Given the notably low electric conductivity along the surface of dielectrics, surface charges are typically regarded as immobile.

1.4 Photoionization models

1.4.1 Photoionization model in air

Photoionization plays a crucial role in the propagation of positive streamers in air. Zheleznyak introduced a computational model, for this process in air based on evaluation of

an integral [70], where parameters of this model are fitted against experimental data [71–74]. In this model, the primary UV radiation source is assumed to be the excited singlet states of N_2, particularly radiative transitions of $b^1\Pi_u$, $b'^1\Sigma_u^+$ and $c_4'^1\Sigma_u^+$ to the ground state $N_2(X^1\Sigma_g^+)$. Corresponding wavelengths are between 98 and 102.5 nm, where predominant absorber in air is O_2. The 102.5 nm wavelength aligns with the ionization threshold energy of oxygen, while the lower bound to this wavelength range is determined by the absorption threshold of N_2 molecules. Intriguing aspects of this process has been discussed in [70, 75]: Essentially, the asymmetry between the excitation and radiation mechanism of N_2 states makes the absorption of photons in this wavelength window by N_2 negligible. Here's why: in streamer scenario the temperature for population of vibrational levels of N_2 is rather low, and so the majority of N_2 molecules in the gas occupy the zeroth vibrational level $X^1\Sigma_g^+(v''=0)$. On the other hand, in the process of excitation of $N_2(X^1\Sigma_g^+,v''=0)$ to the singlet states, these are created *with* vibrational excitation. Then photons emitted from these excited states have particular energies that can be absorbed back only by vibrationaly excited ground states $N_2(X^1\Sigma_g^+,v''>0)$. Because of the overwhelming abundance of $N_2(X^1\Sigma_g^+,v''=0)$, these photons pass through the N_2 practically unnoticed. The absorption by $N_2(X^1\Sigma_g^+,v''=0)$ becomes possible only at wavelengths shorter than 98 nm, which shuts down the absorption window for photoionizing radiaion in air.

According to the Zheleznyak's model [70], the photoionization rate at the point $\mathbf{r}$ due to photons emitted from elementary source volumes $\mathrm{d}V'$ located at $\mathbf{r}'$ is given by an integral:

$$S_{\mathrm{ph}}(\mathbf{r}) = \iiint_{V'} \frac{I(\mathbf{r}')g(|\mathbf{r}-\mathbf{r}'|)}{4\pi|\mathbf{r}-\mathbf{r}'|^2}\,\mathrm{d}V', \tag{1.22}$$

The photon production rate, represented by $I(\mathbf{r}')$ is assumed to be proportional to the local ionization rate $S_i(\mathbf{r}')$. For convenience it is expressed as a function of pressure p in a form:

$$I(\mathbf{r}') = \frac{p_{\mathrm{q}}}{p+p_q}\left(\xi\frac{\nu_u}{\nu_i}\right) S_i(\mathbf{r}'), \tag{1.23}$$

where p_{q} is the quenching pressure at which the rates of radiative de-excitation and collisional quenching are equal, namely for air $p_{\mathrm{q}} = 4000\,\mathrm{Pa}$. The function $g(R)$ in (1.22) is defined by

$$\frac{g(R)}{p_{O_2}} = \frac{\exp(-\chi_{\min}p_{O_2}R) - \exp(-\chi_{\max}p_{O_2}R)}{p_{O_2}R\ln(\chi_{\max}/\chi_{\min})}, \tag{1.24}$$

where $R = |\mathbf{r}-\mathbf{r}'|$, $\chi_{\min} = 0.0262\,\mathrm{Pa}^{-1}\,\mathrm{m}^{-1}$, $\chi_{\max} = 1.5\,\mathrm{Pa}^{-1}\,\mathrm{cm}^{-1}$, and where $p_{O_2} = 2\times 10^4\,\mathrm{Pa}$ is the partial pressure of molecular oxygen at atmospheric pressure. Moreover, the term $(\xi\nu_u/\nu_i)$ represents the product of the photoionization efficiency parameter ξ, and the ratio between the effective electron impact excitation frequency ν_u for photoionizing N_2 states, and the ionization frequency ν_i. It's worth noting that the term $(\xi\nu_u/\nu_i)$ is provided as a function of the reduced electric field in [70, 76], for further discussion see [75, 77, 78].

Steady state assumption behind the Zheleznyak's photoionization model

It's important to understand that Zheleznyak's model adopts a steady-state assumption regarding the population of the emitting excited states. This simplification is reflected by the pressure factor in Eq. (1.23). Indeed, when considering the number density of the

radiative state $[S^*]$, its governing equation is expressed as [78]:

$$\frac{d[S^*]}{dt} = G - \frac{[S^*]}{\tau_0} - \sum_i k_i[S^*][Q_i]. \tag{1.25}$$

Here, G represents the excitation source term, τ_0 is the radiative lifetime, and k_i is the quenching rate for quencher i with number density $[Q_i]$; the summation covers all possible quenchers. The stationary radiation rate is then given by:

$$\frac{[S^*]}{\tau_0} = \frac{G}{1 + \tau_0 \left(\sum_i k_i[Q_i]\right)}. \tag{1.26}$$

Expressing the sum in terms of composition fractions f_i and incorporating the total pressure, p, of the gas using the ideal gas law, we get:

$$\sum_i k_i[Q_i] = \frac{p}{kT} \sum_i k_i f_i. \tag{1.27}$$

By defining the quenching pressure as the pressure under which half of the excited states $[S^*]$ results in radiation and half is lost due to collisional quenching, i.e.,

$$p_q = \frac{kT}{\tau_0 \left(\sum_i k_i f_i\right)}, \tag{1.28}$$

the stationary radiation rate can be reformulated as:

$$\frac{[S^*]}{\tau_0} = G \frac{p_q}{p_q + p}. \tag{1.29}$$

This finally clarifies the pressure factor in Eq. (1.23).

Note that, the validity of the steady-state assumption is predominantly justified at lower pressures, such as those found at sprite altitudes [75]. However, caution is needed at air pressures exceeding p_q. Here, the lifetime of the emitting N_2 states might align closely with the variation timescale of physical parameters in the streamer head. Consequently, under these conditions, omitting the full dynamics of N_2 emissions can lead to significant deviations [75].

1.4.2 Photoionization models in N_2,O_2,CO_2 and He

The photoionization models for air, N_2, O_2 and CO_2 have been thoroughly analyzed in [78]. It was also suggested there that for pure O_2 or N_2, the ionizing radiation may primarily originate from a single electron impact: this can be due to direct dissociative excitation, leading to states O_I and N_I, or due to direct ionizing excitation to the corresponding states O_{II} and N_{II}. This excitation is then followed by a radiative transition of the excited neutral atom or ion. Moreover, it is concluded there that model given by Zheleznyak leads to a reasonable description of photoionization experiments in air; and [78] also provides generalization of Zheleznyak's model for arbitrary N_2–O_2 mixtures and CO_2.

Another major step in photoionization models was a work of Janalizadeh and Pasko [79] that provided a framework for development of photoionization model in non-thermal gas discharges for multicomponent gasses. An example of application of this generalized framework is a model developed for photoionization of metals deposited in the lower ionosphere as a result of meteoric ablation and photodetachment of electrons from negative ions of the Earth's ionosphere due to sources of emission other than solar radiation, see [80].

1.4.3 Photoionization models for helium plasma jets

Photoionization model in the context of atmospheric helium plasma jets was proposed by Naidis in [81]. Regarding the photoionization mechanism at atmospheric pressure Helium, the primary source of ionizing radiation comes from the helium excimer, denoted as He_2^*. This excimer is formed mainly through three-body conversion reactions. Specifically, excited helium atoms (He*) react in the presence of a third body, M, according to the equation:

$$\mathrm{He}^* + \mathrm{He} + M \rightarrow \mathrm{He}_2^* + M.$$

One significant feature of the excimer emission is that it doesn't undergo resonant reabsorption. As a result, it can produce non-local ionization. On the other hand, the resonance radiation emitted by excited helium atoms does experience reabsorption. This is due to the prevailing presence of ground state He atoms, which trap this radiation. Note that in a typical plasma jet setup that is operating at atmospheric pressure [82] have confirmed that helium excimer radiation indeed predominantly drives the photoionization process. This process is crucial for the propagation of the ionization front both within the tube and in the plume. However, it's also worth noting that the current models describing the photoionization effects of helium excimer radiation on molecules like nitrogen, oxygen, and water are somewhat basic. Specifically, they may not fully capture the intricate wavelength dependencies inherent to absorption and photoionization processes [81]. Naidis' He photoionization model was then fitted with a single absorption length in [83] to be applied within the radiative transfer computational framework of [77]; later, the same framework was also used in our work [6]. Only very recently, a refined model for photoionization of air impurities in helium was proposed by Janalizadeh and Pasko in [84].

1.4.4 Kinetic photoionization models

Another class of photoionization models adopts simplified kinetics for the emitting species. For instance, Babaeva et al. [85] used $N_2(b^1\Pi, b'^1\Sigma)$ states. Similarly, Stephens et al. [86] developed a kinetic model for photoionization in air which includes $c_4{}'^1\Sigma_u^+(0)$, $c_4{}'^1\Sigma_u^+(1)$, and $b^1\Pi_u(1)$ emissions. A comparative analysis of this model with Zheleznyak's integral model can be found in Marskar [87]. On the other hand, there also exist stochastic models of photoionization that mimic the Zheleznyak's integrals. These models mimic the propagator by using appropriate absorption function μ and are used to study stochastic effects related to the photoionization [87, 88]. See Marskar's paper [87] for discussion on comparing the Stephens' [86] and Zheleznyak's model. Three-dimensional kinetic modeling of streamer propagation in a nitrogen/helium gas mixture is presented in [89].

1.4.5 Approximate methods for radiative transfer equation

The photoionization model basically provides electrons and ions as a source terms in continuity equations (1.1). The Zheleznyak's integral approach involves calculating the photoionization source at each point of the computational domain by summing the radiation contributions from all other points in the domain. However, this approach may prohibitively escalate the computational costs. Given these challenges, alternative strategies have emerged [77, 90, 91]. These are relying on approximate methods for the solution

of the radiative transfer equation and offer computationally efficient alternatives for calculating photoionization in streamer models. Basic overview of several methods for the solution of approximate radiative transfer equation (RTE), namely Helmholtz and Discrete Ordinate methods are presented here, the following paragraphs are adapted from our work [9] (listed also in selected publications as (B7)).

Let us consider a typical streamer velocity of 10^6 m/s, which is negligibly small compared to the speed of light, then the photon propagation can be regarded as instantaneous and described by the time-independent radiative transfer equation (RTE) [92, 93]:

$$\mathbf{s}\cdot\nabla I_\nu(\mathbf{r},\mathbf{s}) = h\nu c\,\eta_\nu(\mathbf{r},\mathbf{s}) - \mu_\nu I_\nu(\mathbf{r},\mathbf{s}) - \sigma_\nu I_\nu(\mathbf{r},\mathbf{s}) + \frac{\sigma_\nu}{4\pi}\int_{4\pi}\Phi_\nu(\mathbf{s},\mathbf{s}')\,I_\nu(\mathbf{r},\mathbf{s}')\,\mathrm{d}\Omega',$$

which may be rewritten in terms of the photon distribution $\Psi_\nu = (h\nu c)^{-1} I_\nu$:

$$\mathbf{s}\cdot\nabla\Psi_\nu(\mathbf{r},\mathbf{s}) = \eta_\nu(\mathbf{r},\mathbf{s}) - \mu_\nu\Psi_\nu(\mathbf{r},\mathbf{s}) - \sigma_\nu\Psi_\nu(\mathbf{r},\mathbf{s}) + \frac{\sigma_\nu}{4\pi}\int_{4\pi}\Phi_\nu(\mathbf{s},\mathbf{s}')\,\Psi_\nu(\mathbf{r},\mathbf{s}')\,\mathrm{d}\Omega',$$

where I_ν is the specific intensity (physical units J s^{-1} sr^{-1} Hz^{-1} m^{-2}) for the photon frequency ν, h is the Planck constant, c is the speed of light, $\mathbf{r}$ is the position vector, $\mathbf{s}$ is the unit direction vector, η is the added numbers of photons due to emission per unit volume per unit solid angle in the direction $\mathbf{s}$ per unit length, μ is the absorption coefficient, σ is the scattering coefficient and the integral in the last term is the number of scattered photons to the direction $\mathbf{s}$ from all other directions, with $\Phi(\mathbf{s},\mathbf{s}')$ representing the probability that a photon from direction $\mathbf{s}'$ scatters to the direction $\mathbf{s}$. A large family of approximative methods has been developed to eliminate the angular dependence of radiation intensity by expanding it into a limited number of functions $I^i_\nu(\mathbf{r})$. These methods include the P_N approximation, the simplified-P_N (also called SP_N) approximation, and the Discrete Ordinates (DO) method, also referred to as the S_N approximation [93].

The P_N and SP_N approximations expand the radiation intensity in series involving spherical harmonics, then integrate them over all directions, and, by making use of orthogonal properties of spherical harmonics, obtain a set of simultaneous partial differential equations [94]. On the other hand, the S_N approximation discretizes the angular dependence of RTE to obtain a similar set of partial differential equations [95].

Eddington approximation

One of the simplest and widely used approximations of RTE is the first-order approximation of the P_N method, denoted P_1 [93]. It approximates the photon number density with:

$$\Psi(\mathbf{r},\mathbf{s}) = \frac{1}{4\pi}\left(\Psi_0(\mathbf{r}) + 3\boldsymbol{\Psi}_1(\mathbf{r})\cdot\mathbf{s}\right), \tag{1.30}$$

where Ψ_0 is the isotropic part of the photon number density:

$$\Psi_0 = \int_{4\pi}\Psi(\mathbf{r},\mathbf{s})\,\mathrm{d}\Omega, \tag{1.31}$$

and Ψ_1 is the first order anisotropy correction:

$$\boldsymbol{\Psi}_1 = \int_{4\pi}\Psi(\mathbf{r},\mathbf{s})\,\mathbf{s}\,\mathrm{d}\Omega. \tag{1.32}$$

If we neglect the scattering terms in RTE, which is a common practice for modelling the photoionization in streamers, and construct the zeroth moment of the RTE by integrating the RTE over all directions with the approximation above, the resulting equation yields:

$$\nabla \cdot \mathbf{\Psi}_1 + \mu\Psi_0 = 4\pi\eta, \tag{1.33}$$

and, analogically, the first moment ($\int_{4\pi} \mathbf{s} \ldots \mathrm{d}\Omega$):

$$\frac{1}{3}\nabla\Psi_0 + \mu\mathbf{\Psi}_1 = \mathbf{0}. \tag{1.34}$$

Combining the two equations gives the equation for the isotropic part of the photon number density:

$$\nabla^2\Psi_0 - 3\mu^2\Psi_0 = -12\pi\mu\eta. \tag{1.35}$$

The resulting mathematical equation is the screened Poisson equation, and can be solve using the same numerical methods as ordinary Poisson's equation. We note that this equation is also often called Helmholtz equation in literature (e.g. [77, 93]). We will refer to this approximation as the *Eddington approximation* in accordance with [90].

Discrete Ordinates Method

The Discrete Ordinates (DO) method, also known as the S_N approximation of RTE [93, 95], is widely used in radiative transfer problems in many fields, including heat transfer problems [96], atmospheric sciences [97] and astrophysics [98]. This method involves discretizing the angular space into a finite number of discrete directions, or ordinates, and then solving the resulting partial differential equations separately for each direction. The integrals over the solid angle are replaced by numerical quadratures. Each octant of the complete solid angle 4π is discretized into $N_\theta \times N_\phi$ solid angles, where θ and ϕ are the polar and azimuthal angles. The idea was first suggested by Chandrasekhar in 1960 [92] and was first used in the context of neutron transport theory [95, 99]. Because of the simplicity of the method, it is straightforward to increase the order of the approximation by simply increasing the number of discrete directions. The DO method has several advantages over other numerical methods for solving the RTE, including accuracy, efficiency, and versatility. It is also relatively easy to implement and can be used to model a wide range of radiative transfer problems, including both thermal and non-thermal radiation. The discrete ordinates method may be formulated in terms of finite volume method (FVM) [100]. This approach offers benefits over a finite-difference approach, e.g., it guarantees conservation of radiative energy and may be used on unstructured grids [101, 102]. On the other hand one, disadvantages of the DO method also exist. Due to practical limitations in angular discretization, artifacts can appear on the computed radiation field. This is referred to as the 'ray effect' and it is demonstrated in figure 1.6.

Links to Zheleznyak's model

To quantify the photon source term in the RTE for air using Zheleznyak's model [70], the source of ionizing photons is assumed proportional to the electron-impact ionization rate S_i:

$$\eta = \int_0^\infty \eta_\nu \mathrm{d}\nu = \frac{k}{4\pi c} S_\mathrm{i}. \tag{1.36}$$

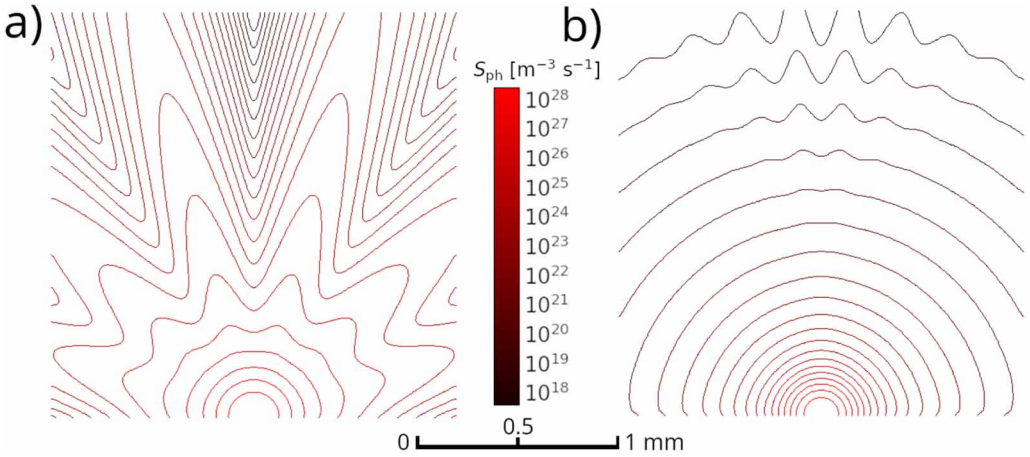

Figure 1.6: Demonstration of the ray effect with different number of discretized directions: (a) $N_\theta \times N_\phi = 3 \times 3$ and (b) $N_\theta \times N_\phi = 12 \times 12$. Figure reprinted from [9].

The proportionality constant k in air depends only weakly on the reduced electric field [70] and the dependence on the pressure in the model can be expressed using (1.23):

$$\eta = \frac{1}{4\pi c} \frac{p_\mathrm{q}}{p + p_\mathrm{q}} \frac{1}{\xi} \left(\frac{\xi}{\gamma} \right) S_\mathrm{i}. \tag{1.37}$$

The dimensionless parameters ξ and γ in air vary slightly with reduced electric field, often approximated by a constant value of $\zeta = \xi/\gamma = 0.06$ as suggested in [103].

The absorption coefficient in air is proportional to the gas number density and since only the oxygen molecules are assumed to be ionized by the radiation of the excited nitrogen state, partial pressure of the oxygen molecules us used:

$$\mu_\nu = \lambda_\nu p_{\mathrm{O}_2}, \tag{1.38}$$

where λ_ν is the mean length of absorption for the frequency ν.

The rate of electron-ion pair production by photoionization is calculated through the number of photons absorbed:

$$S_\mathrm{ph}(\mathbf{r}) = \int_0^\infty \int_{4\pi} \xi_\nu \mu_\nu \Psi_\nu(\mathbf{r}, \mathbf{s}) \, \mathrm{d}\Omega \, \mathrm{d}\nu \tag{1.39}$$

$$= \int_0^\infty \xi_\nu \mu_\nu \Psi_{\nu,0}(\mathbf{r}) \, \mathrm{d}\nu \ , \tag{1.40}$$

where ξ_ν is the ratio of electrons produced by photoionization per photons of frequency ν absorbed and $\Psi_{\nu,0}$ is the isotropic photon number density.

The integral over frequencies is approximated by a sum of contributions from a few frequency bands $\Delta\nu_j$:

$$S_\mathrm{ph}(\mathbf{r}) \approx p_{\mathrm{O}_2} c \sum_j A_j \xi \Psi_{j,0}(\mathbf{r}), \tag{1.41}$$

where the coefficients are manipulated into the weight parameter $A_j = \mu_j \Delta\nu_j \, (p_{\mathrm{O}_2} c)^{-1}$ to obtain the same form as in [77] and the photoionzation efficiency ξ is now considered an effective parameter for the relevant frequency range.

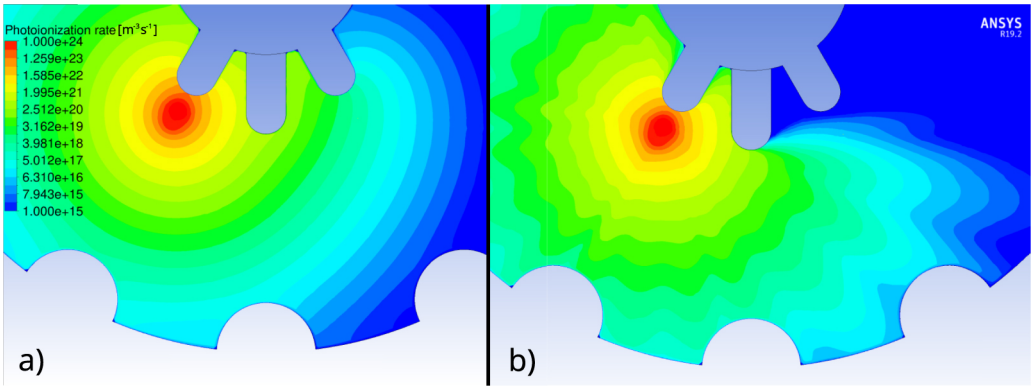

Figure 1.7: Profile of photoionization from a Gaussian profile of ioniazaion (a) the Eddington model with diffuse distribution of photoionization source leaking behind obstacles, and (b) the Discrete Ordinates Method, capturing the photoionization shadow behind obstacles. Figure reprinted from [9].

The resulting equations solved within the Eddington approximation are:

$$\left(\nabla^2 - 3\left(\lambda_j p_{\mathrm{O}_2}\right)^2\right)\left(\xi\Psi_{j,0}\right) = -3\lambda_j p_{\mathrm{O}_2}\frac{q\zeta}{c}S_{\mathrm{i}} \tag{1.42}$$

$$S_{\mathrm{ph}}(\mathbf{r}) = \sum_j S_{\mathrm{ph},j} = p_{\mathrm{O}_2} c \sum_j A_j \xi \Psi_{j,0}(\mathbf{r}), \tag{1.43}$$

where we denote $q = p_{\mathrm{q}}/(p_{\mathrm{q}} + p)$.

For 3 component (3 band) Eddington approximation parameters A_j and λ_j were obtained by [77] by fitting the model proposed in [70]. The same 3 component model is also used for discrete ordinates method where the RTE for jth frequency component is multiplied by $p_{\mathrm{O}_2} c A_j \xi$ to solve directly for the photoionization source component $S_{\mathrm{ph},j}$. If we neglect the scattering terms, as in the case of the Eddington approximation, the discrete ordinates RTE for kth direction is:

$$\mathbf{s}^k \cdot \nabla S^k_{\mathrm{ph},j}(\mathbf{r}) = \frac{p_{\mathrm{O}_2} A_j \zeta q}{4\pi} S_{\mathrm{i}}(\mathbf{r}) - \lambda_j p_{\mathrm{O}_2} S^k_{\mathrm{ph},j}(\mathbf{r}). \tag{1.44}$$

Note that the DOs method offers considerable advantages over the Eddington approximation in cases where radiation shadows need to be captured, see figure 1.7. This is particularly important for accurate simulation of the streamer inception and dynamics as we presented in our work [9], also listed among the selected publication as:

(B7) Jan Tungli, Miroslav Horký, Stanislav Kadlec, and **Zdeněk Bonaventura**. Capturing photoionization shadows in streamer simulations using the discrete ordinates method. *Plasma Sources Science and Technology*, 32(10):105009, 2023. doi: 10.1088/1361-6595/acfcd8.

1.5 Numerical challenges of fluid streamer modelling

Streamer discharges exhibit an inherently multi-scale character in both space and time. The modelling of ionization front's propagation (at atmospheric pressure) requires micrometer space resolution, because the local electrostatic screening length (10^{-6} m) needs to be resolved, while the propagation usually take place over centimeter-scale gaps. As

a result, the simultaneous resolution of extremely fine and large spatial structures is needed. Similarly, the governing time scales span many orders of magnitude: electron-impact ionization and dielectric relaxation occur on the order of 10^{-14}–10^{-12}s, while the overall streamer evolution lasts over nanoseconds. In more complex scenarios such as repetitively pulsed or AC-driven discharges, this multi-scale character is even more pronounced. Fast streamer dynamics lasting a few nanoseconds are followed by post-discharge phases extending over microseconds, during which slower processes dominate: ion-ion recombination, electron attachment and detachment, diffusion, neutral gas heating and convection. Capturing the full discharge/post-discharge cycle requires numerical methods that remain efficient and accurate across several orders of magnitude of temporal and spatial scales. Classical fluid models solve drift–diffusion equations for electrons and ions, coupled with Poisson's equation for the electric field, as described in Section 1.1. Traditional approaches either rely on restrictive explicit time stepping, constrained by the smallest physical scales, e.g. [104], or on semi-implicit decoupling schemes whose accuracy is difficult to quantify, e.g. [105]. Existing adaptive local time-stepping techniques improve efficiency, but still lack rigorous global error control, particularly in the coupling between transport and electric field computation. Our paper

(B1) Max Duarte, **Zdeněk Bonaventura**, Marc Massot, Anne Bourdon, Stéphane Descombes, and Thierry Dumont. A new numerical strategy with space-time adaptivity and error control for multi-scale streamer discharge simulations. *Journal of Computational Physics*, 231(3):1002–1019, 2012. doi: 10.1016/j.jcp.2011.07.002,

addresses these limitations by introducing a new numerical strategy that combines second-order time adaptive integration, space-adaptive multiresolution, and rigorous error control. The method decouples the electric field and drift–diffusion equations while guaranteeing second-order accuracy through embedded error estimators. A Strang-splitting time integration scheme equipped with dedicated high-order solvers handles the multiscale reaction, diffusion, and convection processes [106]. Meanwhile, adaptive mesh refinement strategy grounded in wavelet analysis [107, 108], is ensuring fine resolution only where steep gradients or strong reactive fronts occur. The key idea behind multiresolution adaptivity is to represent the solution on a hierarchy of nested dyadic grids and to measure local spatial regularity using *details*: wavelet-based coefficients obtained from inter-level prediction. Where details remain below user-specified thresholds, the solution is sufficiently smooth and the local grid can be coarsened; where they exceed the threshold, the grid is refined. This adaptive mechanism provides rigorous control of the approximation error while ensuring that the spatial resolution automatically follows steep gradients, propagating fronts, or localized structures typical of plasma discharges. Because the underlying multiresolution transform is independent of the governing equations, the method offers a mathematically clean and general framework for generation of adaptive grids, achieving substantial data compression without sacrificing conservation, accuracy, or stability. This unified spatially and temporally adaptive framework provides a controlled, accurate, and computationally efficient way to simulate streamer propagation in repetitively pulsed discharges.

One of the key challenges was to develop a Poisson solver on dynamically adapted grids, basic idea behind the Poisson's equation representation via finite-volume method was described in Section 1.2. The same finite-volume strategy was extended to multidimensional case in the framework of the Finite-Volume Multiresolution Method (FVMM) and presented in our work

(B3) Max Duarte, **Zdeněk Bonaventura**, Marc Massot, and Anne Bourdon. A numerical strategy to discretize and solve the poisson equation on dynamically adapted multiresolution grids for time-dependent streamer discharge simulations. *Journal of Computational Physics*, 289:129–148, 2015. doi: 10.1016/j.jcp.2015.02.038.

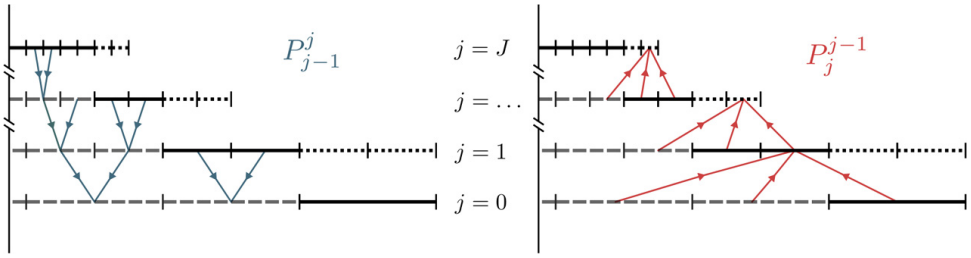

Figure 1.8: Part of a one-dimensional graded tree indicating the leaves (solid lines) that form the adapted grid, as well as the inner (dashed lines) and ghost (dotted lines) cells. Projection P_{j-1}^{j} (left) and prediction P_{j}^{j-1} (right) operations are also represented. Figure reprinted from [11].

In particular, we investigated the influence of data compression on the accuracy of approximations obtained for Poisson's equation. A key novelty of this approach, in the context of elliptic solvers on adapted grids, was that instead of solving the discrete equations level-wise across the hierarchy of embedded grids, we devised a numerical procedure that represents the elliptic operators directly on the adapted grid, i.e. on a mesh composed of cells with varying spatial resolution. The algorithm relies on a local reconstruction of uniform-grid zones at inter-level interfaces by means of multiresolution operations between consecutive grid levels, see figure 1.8, ensuring the conservation and accuracy properties of multiresolution schemes. This approach yields a standalone algebraic system that is completely independent of the adaptive meshing strategy, its data structure, and the numerical integration of the time-dependent PDEs associated with the model. The resulting discrete system, see figure 1.9 can therefore be solved in a single step over the entire computational domain, without requiring grid overlap, by employing an appropriate linear solver.

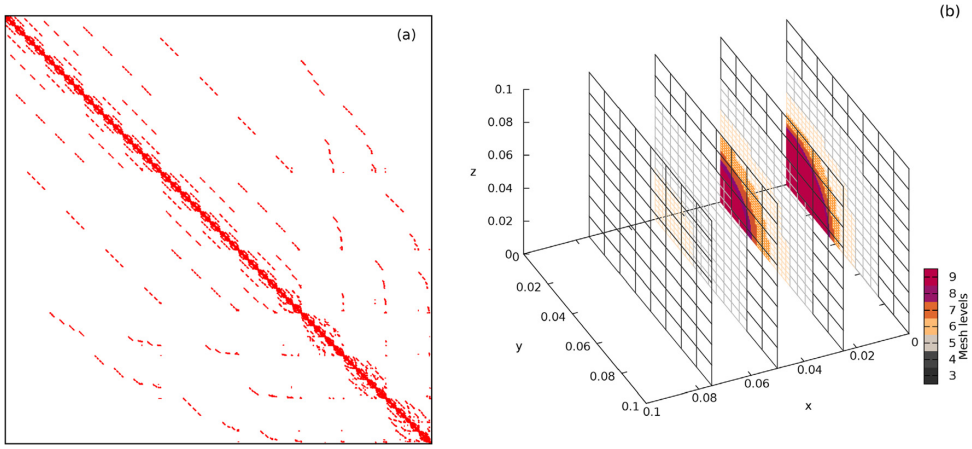

Figure 1.9: (a) Structure of the discrete Laplacian $\mathcal{A}$ on a three-dimensional multiresolution grid; (b) cutting planes through the adapted mesh for maximum level of refinement $J = 9$, and multiresolution threshold $\eta_{\mathrm{MR}} = 10^{-4}$. Figures reprinted from [11].

Finally, in our third contribution we applied the complete adaptive framework to a physically important problem: determining the conditions under which two streamers interact and merge. The multiresolution strategy allowed us to resolve simultaneously the fine structure of each streamer head and the larger-scale electric field coupling between them, while the adaptive time integration accurately captured their short-lived interaction dynamics, see figure 1.10.

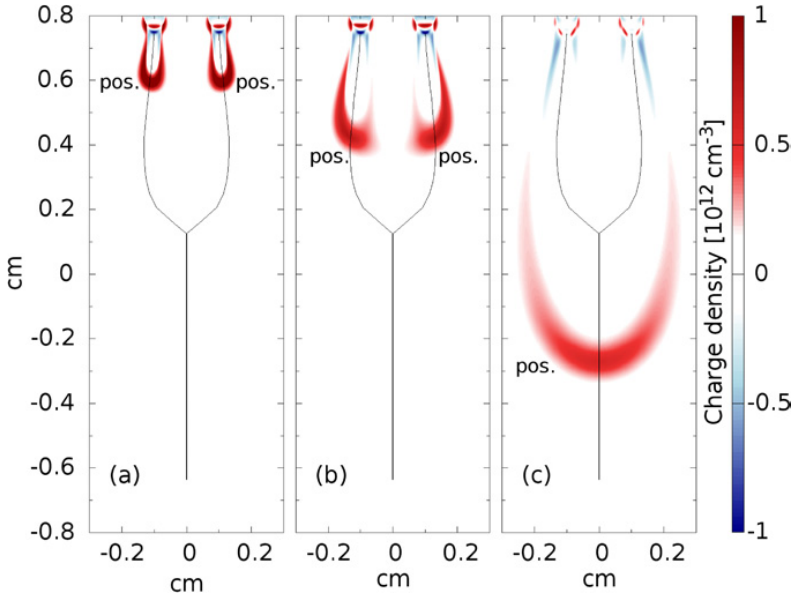

Figure 1.10: Time evolution of the net charge density for two positive streamers at ground pressure for an applied electric field $E_a = 1.5E_{\text{cbf}}$ from two Gaussian seeds. (a) t = 5.0 ns: well-developed streamers repulsing each other, (b) t = 6.3 ns: transition between repulsion and merging, (c) t = 8.0 ns: propagation of a single discharge. Figure reprinted from [12].

Using this capability, we performed a systematic parametric study and derived a quantitative merging criterion based on the ratio of streamer head separation to the characteristic ionization-region width. Our study, published in

(B2) **Zdeněk Bonaventura**, Max Duarte, Anne Bourdon, and Marc Massot. Derivation of a merging condition for two interacting streamers in air. *Plasma Sources Science and Technology*, 21(5):052001, 2012. doi: 10.1088/0963-0252/21/5/052001.

highlights the strength of the adaptive methodology: high-resolution simulations are feasible which would be computationally prohibitive on uniform grids and allows physically grounded conclusions to be drawn from fully resolved streamer–streamer interaction.

1.6 Runaway electrons

In 1924 the Nobel priced physicist C.T.R. Wilson predicted that there is a possibility of large scale discharges high above thunderclouds. He recognized that if the dipole electric field of a thundercloud vanishes as the inverse third power of the distance from the thunderclouds, while the critical field falls exponentially with altitude as the air density decreases, then there must be an altitude high above, where the electric force would

exceed the 'sparkling' limit [109]. As a result, one may expect that large scale discharges can be formed also at high altitudes. And indeed, *transient luminous events*, see figure 1.11, has been finally recorded some 75 years later [110]. Wilson also predicted that

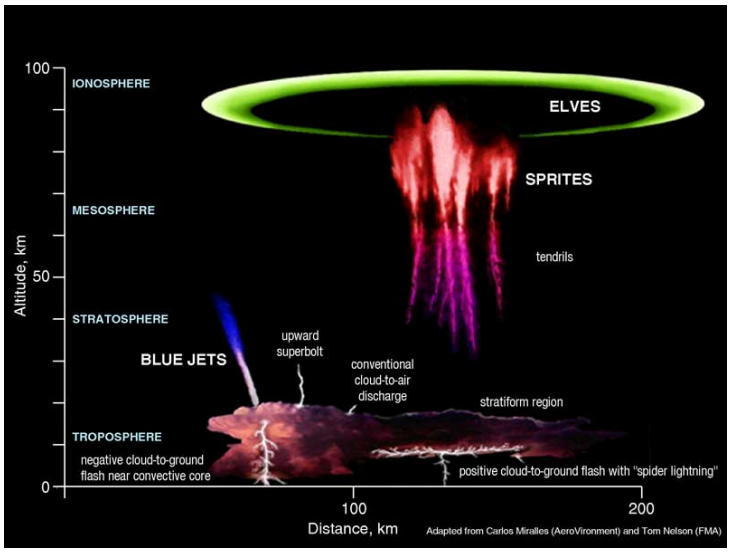

Figure 1.11: An illustration of different kinds of transient luminous events (TLEs). Credits: National Oceanic and Atmospheric Administration (NOAA), `https://www.nssl.noaa.gov/education/svrwx101/lightning/types/`

large scale thundercloud fields are able to accelerate electrons to high energies. These so called *runaway electrons* (RE) arise in cases when the accelerating force of thunderstorms' electric fields exceeds the effective collisional friction experienced by electrons as they interact with air molecules.

The figure 1.12 shows the rate of energy loss for an electron moving in air in terms of the *dynamic friction force*. The solid curve is the friction force due to scattering of

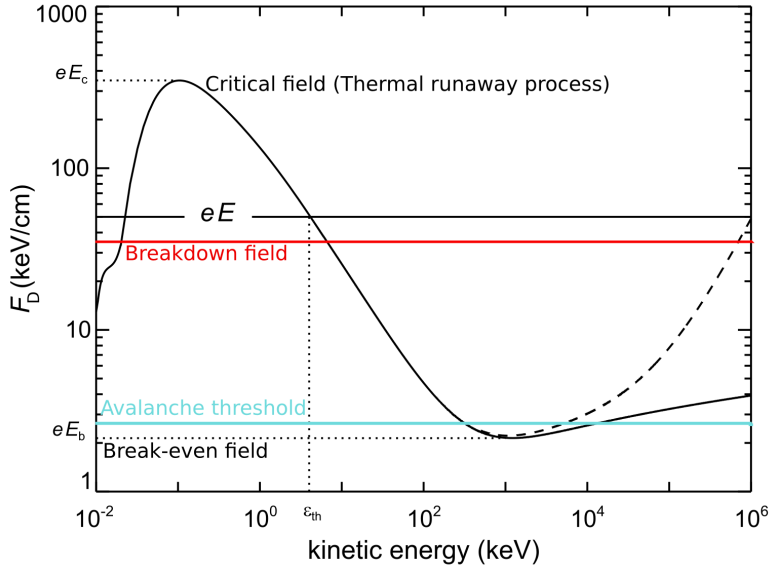

Figure 1.12: The effective frictional force experienced by a free electron (or positron) moving through air at STP as a function of kinetic energy. Adapted from [111]

electrons with air molecules, while the dashed curve is the effect of bremsstrahlung emission. The horizontal line shows electric force eE accelerating the electrons. At the given electric field the runaways occur for kinetic energies higher than some threshold ε_{th}. The minimum field for RE to appear is so called break-even field which is associated with the minimum friction force at electron energy of about 1 MeV. On the other hand, for fields higher than the maximum friction force, all low energy (thermal) electron population eventually runaways. This is referred to as the *thermal runaway process*.

In 1992 Gurewich discovered that adding Møller scattering to possible processes, REs in air may undergo significant multiplication resulting in *Relativistic Runaway Electron Avalanche* (RREA) [112], with an increase in the number of runaway electrons of up to 10^5 over the Wilson runaway electron mechanism. Later on, Joe Dwyer [113] showed that including X-ray interactions and positrons may lead to secondary avalanches resulting in so called *relativistic feedback* with an increase in the number of runaway electrons of up to 10^{13} over the RREA mechanism.

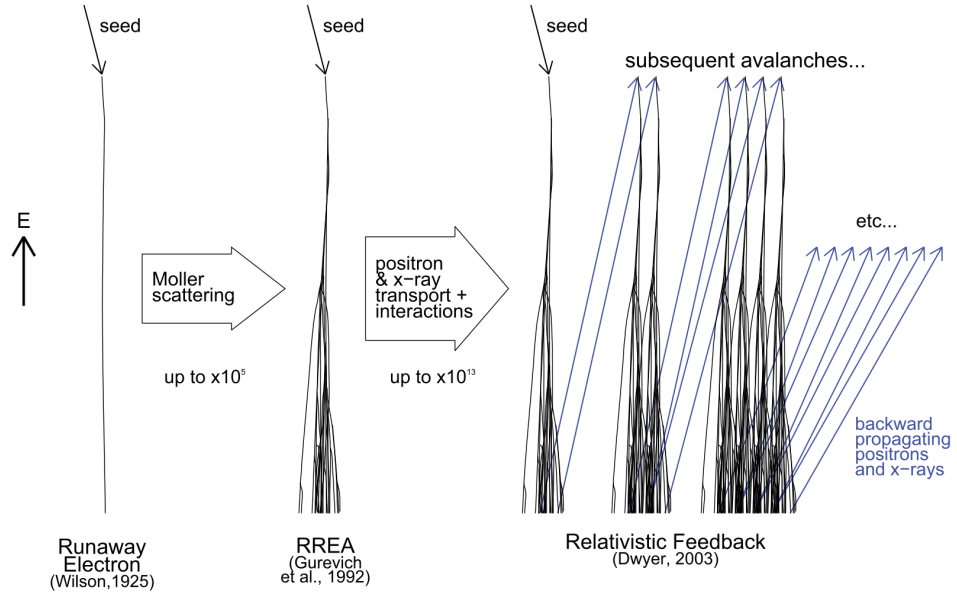

Figure 1.13: Mechanisms for generating energetic electrons in an atmosphere. Figure adapted from [111].

In the same time, sub-ms duration bursts of photons from thunderstorms with energies reaching above 20 MeV, the Terrestrial Gamma-ray Flashes (TGFs), were first observed in 1991 by the Compton Gamma-Ray Observatory, when the satellite was located above thunderstorms [114]. TGFs are proposed to be bremsstrahlung from high-energy electrons accelerated in thunderstorm electric fields [111]. The acceleration mechanism, and its relation with lightning and TLEs, is still debated.

Electric fields of thunderstorms exist on several spatial and temporal scales. On the smallest scale there is the field of the streamer tip. Then follows the field around a leader as in the lightning or a in a blue jet. On even larger scale, there exists space charge field in the thunderstorm clouds and finally, the impulsive fields generated by lightning discharges reaching from the clouds to the ionosphere. The challenge is to identify a plausible combination of those fields that will create pulses of high-energy electrons which, in turn, generate photon pulses that match TGF observations. Theories to explain TGFs build on the Wilson's runaway electrons amplified through the RREA and relativistic feedback

mechanisms. All these theories require seed electrons with energies in the runaway regime.

In our paper

(B4) Olivier Chanrion, **Zdeněk Bonaventura**, Deniz Çinar, Anne Bourdon, and Torsten Neubert. Runaway electrons from a 'beam-bulk' model of streamer: application to TGFs. *Environmental Research Letters*, 9(5):055003, 2014. doi: 10.1088/1748-9326/9/5/055003.

we addressed the electron acceleration in the streamer region of lightning. We presented the first 'beam-bulk' model of self-consistent streamer dynamics and electron acceleration. The model combines a Monte Carlo Collision code [54] that simulates the high-energy electrons (100 eV) and a fluid code that simulates the bulk of the low-energy electrons and ions. For a negative streamer discharge, we showed how electrons are accelerated in the large electric field in the tip of the streamer and travel ahead of the streamer where they ionize the gas, see figure 1.14. In comparison to the results obtained with a classical fluid model for a negative streamer, the beam-bulk model predicts a decrease of the magnitude of the peak electric field and an increase of the streamer velocity. Furthermore, we show that a significant number of runaway electrons is lost by diffusion outside of the streamer tip.

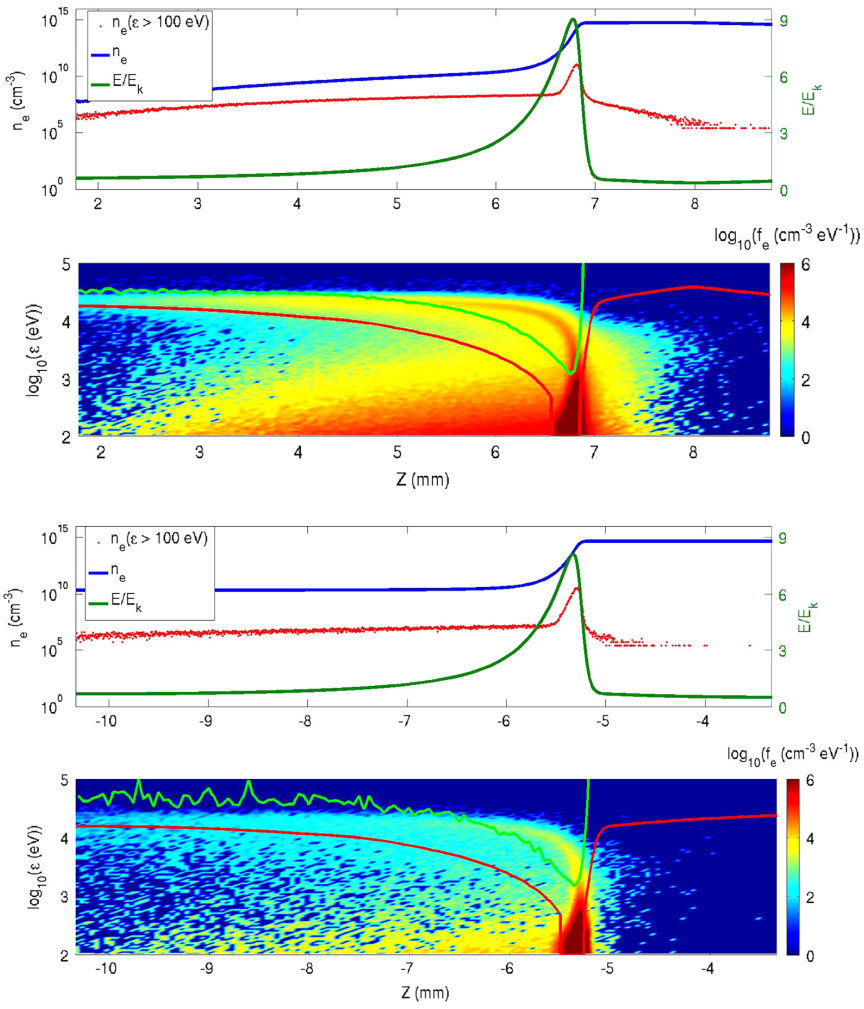

Figure 1.14: Beam-bulk simulations for an applied voltage of (top) and (bottom) at ns. The total electron density (blue), the high-energy electron density (red) and the electric field normalized by the conventional breakdown field (green) are shown on the top of the two sub-panels, and on the bottom panel the space-energy electron distribution together with the energy threshold for runaway (red line). Green line shows the effective friction force. Reprinted from [7].

In order to grasp the diffusive losses of runaway electrons we focused on the runaway threshold definition with a particular interest in the influence of the angular scattering, for electron energy close to the runaway threshold.

In our work

(B5) Olivier Chanrion, **Zdeněk Bonaventura**, Anne Bourdon, and Torsten Neubert. Influence of the angular scattering of electrons on the runaway threshold in air. *Plasma Physics and Controlled Fusion*, 58(4):044001, 2016. doi: 10.1088/0741-3335/58/4/044001.

we compared the outcome of different scattering models based on the solution of either Fokker-Planck equation, or on test particle Monte Carlo Collision approach, with increasing complexity in the description of the electrons scattering. Example of electron orbits in the phase space based on Fokker-Planck equation with forward scattering are shown in figure 1.15. The results show that the inclusion of the stochastic nature of collisions smooths the probability to run away around the threshold. Furthermore, we observed that a significant number of electrons diffuse out of the runaway regime when we take into account the diffusion in angle due to the scattering. Those results suggested that runaway threshold energy based on the Fokker-Planck model—with the assumption of the angular equilibrium—is about 1.6 to 1.8 times higher than the one proposed by [115, 116], depending on the magnitude of the ambient electric field. The threshold obtained is also found to be 5 to 26 times higher than the conventional runaway threshold assuming forward scattering. Furthermore, we have shown that the assumption of forward scattering is not valid below 1 MeV where the runaway threshold usually is defined.

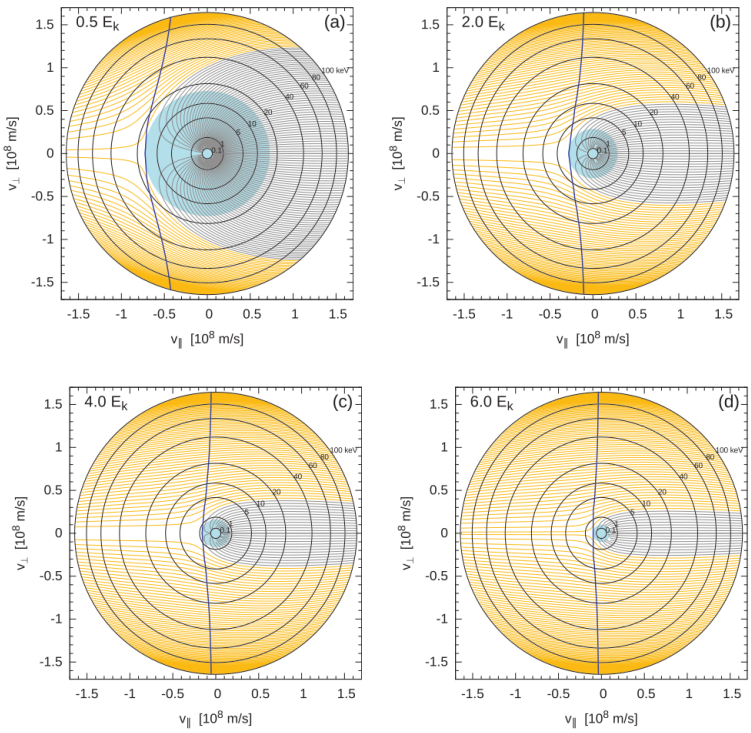

Figure 1.15: Orbits of the Fokker-Planck equation with forward scattering for electric fields of 0.5, 2, 4, and 6E$_k$. $v_\parallel = v\mu$ and $v_\perp = v\sqrt{1-\mu^2}$ (where μ is the cosine of the angle between the electric field and the electron momentum vector) are parallel and perpendicular components of the electron velocity with respect to the electric field. Golden orbits run away, while the thin blue orbits are trapped. The golden orbits accelerate when $-F_D - eE\mu > 0$, and the borderline for this condition is shown by the thick blue line. The light blue circle zone in the center covers energies that are below the runaway threshold $\varepsilon_{\mathrm{th}}$, and all electron orbits entering this zone are trapped. Reprinted from [8].

Chapter 2

Models for electric field determination from optical emissions in streamers

Knowledge of the mean electron energy and electric field in industrial plasma discharges is crucial for optimization of many applications, such as plasma surface treatment, air flow control or plasma-assisted combustion [117–119]. Multiple methods for the determination of these crucial plasma parameters have been developed so far, for different plasmas in various gas mixtures [120–122]. Methods based on optical emission (OE) spectroscopy provide a non-intrusive, in-situ and low-cost alternative to more complex laser-aided methods. Some of these OE spectroscopy methods are sensitive directly to the electric field variations, e.g. methods based on Stark effect [123, 124], yet these techniques are usually limited to certain gases. Another approach is to use intensity ratio of selected atomic lines or spectral bands intensities in combination with simplified collision-radiative models determining the electric field indirectly. The most utilized is probably the ratio of spectral bands intensities of molecular nitrogen [125] or atomic line intensities in helium plasmas [126].

2.1 Generic Formulation of the Ratio Method

To establish the theoretical background, we outline the basic equations underlying the classical ratio method, formulated independently of any specific gas. The method combines balance equations for two excited states, assuming discharge conditions where direct electron-impact excitation of these states dominates, and the effective lifetime of a given state is determined by the total radiative decay rate and by collisional quenching with atoms or molecules in the gas. The balance equation for an excited state $\mathtt{k}$ can then be expressed as

$$\frac{\mathrm{d}n_{\mathtt{k}}}{\mathrm{d}t} = -\frac{n_{\mathtt{k}}}{\tau_{\mathtt{k}}^{\mathrm{eff}}} + \nu_{\mathtt{k}} n_{\mathtt{e}}, \tag{2.1}$$

where $n_{\mathtt{k}}$ is the number density of excited state $\mathtt{k}$, $\nu_{\mathtt{k}}$ the excitation collision frequency by electron impact, $n_{\mathtt{e}}$ the electron number density, and $\tau_{\mathtt{k}}^{\mathrm{eff}}$ is the effective lifetime of the $\mathtt{k}$ state. Note that the excitation collision frequency $\nu_{\mathtt{k}}$ is a known function of the mean

electron energy. Combining balance equations (2.1) for two excited states a and b yields

$$\frac{\dfrac{\mathrm{d}n_{\mathtt{a}}}{\mathrm{d}t}+\dfrac{n_{\mathtt{a}}}{\tau_{\mathtt{a}}^{\mathrm{eff}}}}{\dfrac{\mathrm{d}n_{\mathtt{b}}}{\mathrm{d}t}+\dfrac{n_{\mathtt{b}}}{\tau_{\mathtt{b}}^{\mathrm{eff}}}}=\frac{\nu_{\mathtt{a}}n_{\mathtt{e}}}{\nu_{\mathtt{b}}n_{\mathtt{e}}}=\frac{\nu_{\mathtt{a}}}{\nu_{\mathtt{b}}}=\Theta(\varepsilon), \tag{2.2}$$

where the unknown electron density $n_{\mathtt{e}}$ cancels out, and the $\Theta(\varepsilon)$ is a known function of the mean electron energy. The link between the excited-state populations and measurable quantities is established through the emitted spectral line intensities. The line intensity for a particular transition $j \to k$ and the density of the excited state n_j can be directly linked by the following relation:

$$I_{jk} = n_j A_{jk} hc/\lambda_{jk} = L_{jk} n_j, \tag{2.3}$$

where λ_{jk} is the characteristic wavelength of emitted radiation during the transition between upper j and lower k states, h is the Plank constant, and c is the speed of light, L_{jk} is a proportionality factor for the given transition. Moreover, A_{jk} is the Einstein coefficient for spontaneous emission. Consequently, equation (2.2) expressed in terms of selected line intensities $I_{\mathtt{a}}$ and $I_{\mathtt{b}}$ yields

$$\frac{L_{\mathtt{b}}}{L_{\mathtt{a}}}\frac{\dfrac{\mathrm{d}I_{\mathtt{a}}}{\mathrm{d}t}+\dfrac{I_{\mathtt{a}}}{\tau_{\mathtt{a}}^{\mathrm{eff}}}}{\dfrac{\mathrm{d}I_{\mathtt{b}}}{\mathrm{d}t}+\dfrac{I_{\mathtt{b}}}{\tau_{\mathtt{b}}^{\mathrm{eff}}}}=\Theta(\varepsilon), \tag{2.4}$$

providing experimentally accessible spectroscopic measure of the electron energy or reduced electric field in the plasma, see e.g. [28, 29, 125].

2.2 Influence of streamer geometry and light-detection scenarios

In our paper

(A1) **Zdeněk Bonaventura**, Anne Bourdon, Sebastien Celestin, and Victor P Pasko. Electric field determination in streamer discharges in air at atmospheric pressure. *Plasma Sources Science and Technology*, 20(3):035012, 2011. doi: 10.1088/0963-0252/20/3/035012.

we have discussed different approaches to derive the electric field in positive streamer discharges in air at ground pressure based on the recordings of the emissions of the second positive system (SPS) N_2: $C^3\Pi_u \to B^3\Pi_g$ and first negative system (FNS) N_2^+ : $B^2\Sigma_u^+ \to X^2\Sigma_g^+$. As a test-case, we have considered the propagation of a positive streamer in air at ground pressure and we have computed the spatio-temporal distributions of OEs and electric field in the discharge self-consistently, see figure 2.1. We have shown that the steady-state condition of emitting states $N_2^+(B^2\Sigma_u^+)$ and $N_2(C^3\Pi_u)$ is not fulfilled in air at ground pressure and then its use to determine the local and instantaneous peak electric field in the streamer head may overestimate this field by a factor of 2. However, when spatially and time-integrated OEs are considered, we have shown that it is possible

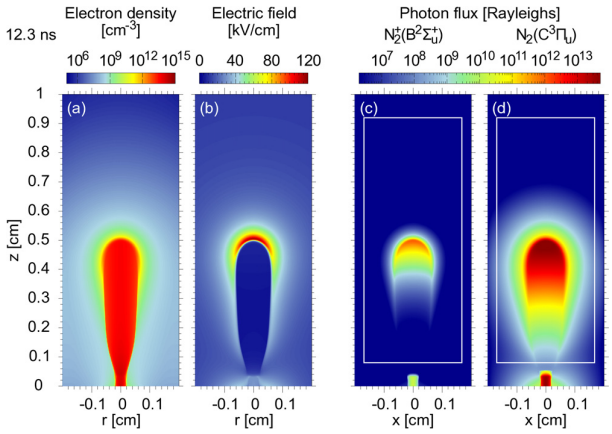

Figure 2.1: Cross sectional views of electron density (a), electric field (b), instantaneous flux of photons (c) and (d) emitted from $N_2^+(B^2\Sigma_u^+)$ and $N_2(C^3\Pi_u)$, respectively, for a horizontal line of sight for a positive streamer at time t = 12.3 ns when the streamer crosse the middle of the simulation domain. The white line in (c) and (d) represents the integration window for the volume integration of instantaneous OEs. Figure reprinted from [2].

to use the steady state equation to accurately determine the peak electric field in an air discharge at atmospheric pressure.

For time-integrated OEs, we have shown that the steady-state equation can be used to derive the electric field in discharges *if the time of integration is sufficiently long* (i.e. at least longer than the longest characteristic lifetime of excited species) to have the time to collect all the light from the emitting zones of the streamer. We have also studied the derivation of the electric field in air discharges at atmospheric pressure using OEs recorded using slits (i.e. a window with a small width but a sufficiently large radial extension to contain the total radial extension of the discharge), see figure 2.2. Our studies demonstrate that spatially integrated OEs over slits can be used with the steady-state equation to determine the electric field. For this case we have also provided a correction factor.

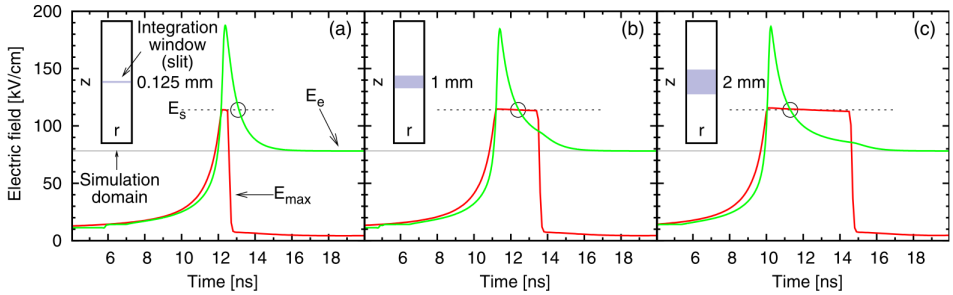

Figure 2.2: Estimation of the peak electric field for slits of different widths. (a) 0.125 mm, (b) 1.0 mm and (c) 2 mm. Red solid line: time-dependent maximum electric field $E_{\max}$ in the field of view of the slit, computed with the discharge code. E_s is the actual peak electric field of the streamer head. Green solid line: electric field derived using time-integrated OEs spatially integrated over the slits in the steady-state equation. E_e is the converged value of the estimated value of electric field. The open circles show the time t for which the estimated electric field is equal to E_s. Figure reprinted from [2].

2.3 Sensitivity analysis and uncertainty quantification of dominant processes for the FNS/SPS ratio method.

The ratio of the spectral band intensities of the first negative and second positive spectral systems of molecular nitrogen is often applied for various plasmas, e.g. barrier and corona discharges for industrial applications or geophysical plasmas occurring in the Earth's atmosphere. The method relies on the dependence of the intensity ratio $R(E/N)$ of selected bands on the reduced electric E/N. There are two ways of obtaining the $R(E/N)$ dependence, either using a theoretical model with appropriate kinetic data or by means of spectroscopic measurements in a known electric field. Precise experimental determination of $R(E/N)$ faces numerous challenges. It has been performed by Paris et al. [127] using non-self-sustaining DC discharge in a parallel-plane gap configuration. The discharge was used for determining $R(E/N)$ dependence in air in the pressure range from 300 to 10^5 Pa. It has also been revealed, that for air discharges at pressures above 10 kPa, the ratio $R(E/N)$ is independent of pressure and is solely a function of E/N [128]. The $R(E/N)$ dependence can also be obtained by using a theoretical model but one has to be aware of the uncertainties in the kinetic data, i.e., reaction rate constants and cross-sections. Several models have been constructed with the purpose of the theoretical determination of the $R(E/N)$, e.g. [129, 130], each of them providing a somewhat different $R(E/N)$, depending on the kinetic data that have been used. In many cases, however, the choice of the kinetic data and the uncertainty of the model are not discussed.

In our work

(A2) Adam Obrusník, Petr Bílek, Tomáš Hoder, Milan Šimek, and **Zdeněk Bonaventura**. Electric field determination in air plasmas from intensity ratio of nitrogen spectral bands: I. Sensitivity analysis and uncertainty quantification of dominant processes. *Plasma Sources Science and Technology*, 27(8):085013, 2018. doi: 10.1088/1361-6595/aad663.

we approached the problem of theoretical $R(E/N)$ determination constructing a well-justified model and providing the $R(E/N)$ with its confidence band. To achieve that, we begin with a 'full kinetic model' of N_2/O_2 plasma comprising of 617 reactions from [131–134] and performed sensitivity analysis on it using the elementary effects method (EEM) [135] to identify the minimal set of reactions important for the FNS/SPS ratio. On this 'reduced model', we have then performed Monte Carlo-based uncertainty quantification in order to provide a confidence band for theoretical $R(E/N)$ dependence and we have also identified main sources of uncertainties. We arrived at the conclusion that the total uncertainty of the $R(E/N)$ curve is several orders in magnitude, see figure 2.3. Knowing that the confidence band is very broad, and knowing the processes which cause the uncertainty, in our work

(A3) Petr Bílek, Adam Obrusník, Tomáš Hoder, Milan Šimek, and **Zdeněk Bonaventura**. Electric field determination in air plasmas from intensity ratio of nitrogen spectral bands: II. Reduction of the uncertainty and state-of-the-art model. *Plasma Sources Science and Technology*, 27(8):085012, 2018. doi: 10.1088/1361-6595/aad666.

we set on a quest of reducing the uncertainty by tracking the historical evolution of the kinetic data, their cross-validation by independent authors and by taking into account

advances in the experimental methods, we separated datasets that have not been rendered inaccurate by later works. By doing so, we reduce the uncertainty of the theoretical $R(E/N)$ dependence and proposed narrower confidence band to be used, see figure 2.4.

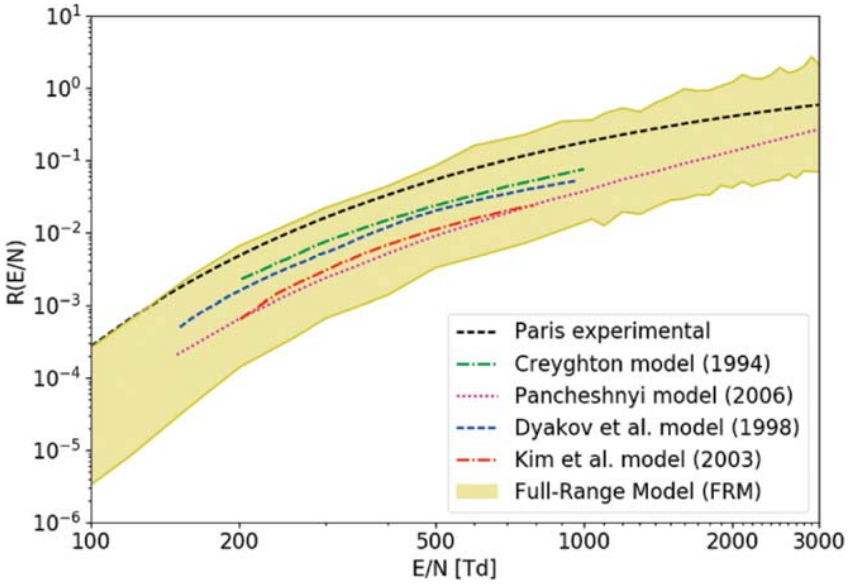

Figure 2.3: Comparison of the total confidence band of the FNS/SPS model with $R(E/N)$ curves published in earlier works. Referenced models: Paris (2005) [128] Creyghton (1994) [129], Pancheshnyi (2006) [130], Dyakov (1998) [136]. Kim (2003) [137], FRM: our work [14].

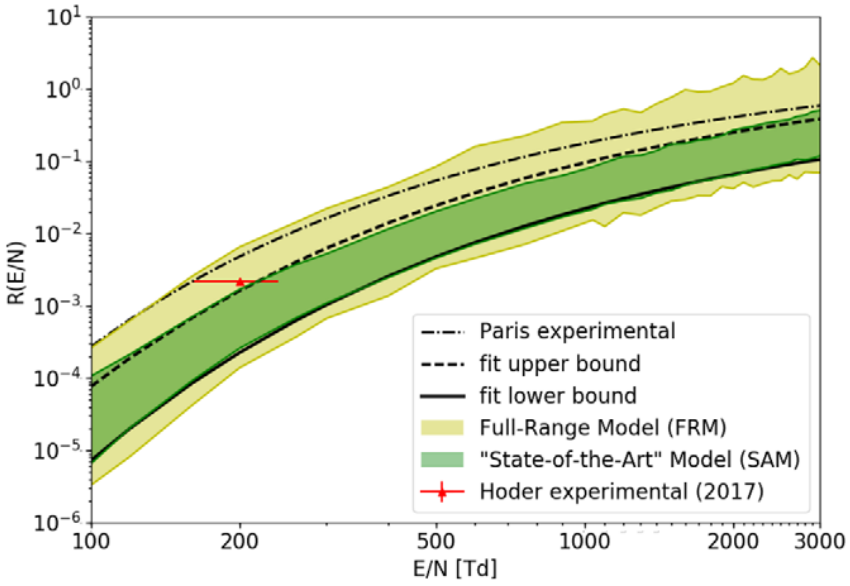

Figure 2.4: Comparison of he FNS/SPS model for the full-range-model (FRM) [14] and 'state-of-the-art' (SAM) [15] model confidence bands. Hoder (2017) [138], Paris experimental [128]

Conclusion and outlook

The contents of this habilitation thesis offers a glimpse into a significant part of the past eighteen years of my scientific life. The physics of streamers, runaway electrons, computational aspects of numerical models, and the unceasing exploration of how the world works, and how it can be described in order to be modelled, have brought me a great deal of joy. Yet the most crucial ingredient of the joyful scientific work is in the collaboration with other people. In this regard, I have been exceptionally fortunate: I have had the opportunity to work with and learn from remarkable colleagues at all stages of their careers: advisors, peers, as well as students.

Many of these collaborations have grown into long-term partnerships, and new unexplored horizons continue to emerge. What are the effects of runaway electrons in triggering negative corona discharge pulses? How do transient sparks interact with the surface of water? How can the ratio method be applied in argon discharges? These questions represent some of the current and future directions of my research.

Bibliography

[1] Milan Šimek, Petr Hoffer, Jan Tungli, Václav Prukner, Jiří Schmidt, Petr Bílek, and Zdeněk Bonaventura. Investigation of the initial phases of nanosecond discharges in liquid water. *Plasma Sources Science and Technology*, 29(6):064001, jun 2020. doi: 10.1088/1361-6595/ab87b7. URL https://doi.org/10.1088/1361-6595/ab87b7.

[2] Zdeněk Bonaventura, Ján Tungli, Petr Bílek, and Milan Šimek. Electron multiplication and avalanching in nanovoids at the initial stage of nanosecond discharge in liquid water. *Plasma Sources Science and Technology*, 30(6):065023, jun 2021. doi: 10.1088/1361-6595/abff73. URL https://doi.org/10.1088/1361-6595/abff73.

[3] Petr Bílek, Ján Tungli, Tomáš Hoder, Milan Šimek, and Zdeněk Bonaventura. Electron–neutral bremsstrahlung radiation fingerprints the initial stage of nanosecond discharge in liquid water. *Plasma Sources Science and Technology*, 30(4): 04LT01, apr 2021. doi: 10.1088/1361-6595/abef18. URL https://doi.org/10.1088/1361-6595/abef18.

[4] Zdeněk Bonaventura, Petr Bílek, Ján Tungli, and Milan Šimek. Analysis of secondary emission mechanism in electron avalanches propagating in cylindrical nanoruptures in liquid water. *Plasma Sources Science and Technology*, 31(3): 035003, mar 2022. doi: 10.1088/1361-6595/ac4ddf. URL https://doi.org/10.1088/1361-6595/ac4ddf.

[5] Mirko Černák, Tomáš Hoder, and Zdeněk Bonaventura. Streamer breakdown: cathode spot formation, trichel pulses and cathode-sheath instabilities. *Plasma Sources Science and Technology*, 29(1):013001, dec 2019. doi: 10.1088/1361-6595/ab5051. URL https://doi.org/10.1088/1361-6595/ab5051.

[6] Pedro Viegas, Elmar Slikboer, Zdenek Bonaventura, Olivier Guaitella, Ana Sobota, and Anne Bourdon. Physics of plasma jets and interaction with surfaces: review on modelling and experiments. *Plasma Sources Science and Technology*, 31(5):053001, may 2022. doi: 10.1088/1361-6595/ac61a9. URL https://dx.doi.org/10.1088/1361-6595/ac61a9.

[7] O Chanrion, Z Bonaventura, D Çinar, A Bourdon, and T Neubert. Runaway electrons from a 'beam-bulk' model of streamer: application to TGFs. *Environmental Research Letters*, 9(5):055003, may 2014. doi: 10.1088/1748-9326/9/5/055003. URL https://doi.org/10.1088/1748-9326/9/5/055003.

[8] O Chanrion, Z Bonaventura, A Bourdon, and T Neubert. Influence of the angular scattering of electrons on the runaway threshold in air. *Plasma Physics and Controlled Fusion*, 58(4):044001, jan 2016. doi: 10.1088/0741-3335/58/4/044001. URL https://doi.org/10.1088/0741-3335/58/4/044001.

[9] Jan Tungli, Miroslav Horký, Stanislav Kadlec, and Zdeněk Bonaventura. Capturing photoionization shadows in streamer simulations using the discrete ordinates method. *Plasma Sources Science and Technology*, 32(10):105009, oct 2023. doi: 10.1088/1361-6595/acfcd8. URL https://doi.org/10.1088/1361-6595/acfcd8.

[10] Max Duarte, Zdeněk Bonaventura, Marc Massot, Anne Bourdon, Stéphane Descombes, and Thierry Dumont. A new numerical strategy with space-time adaptivity and error control for multi-scale streamer discharge simulations. *Journal of Computational Physics*, 231(3):1002–1019, 2012. ISSN 0021-9991. doi: https://doi.org/10.1016/j.jcp.2011.07.002. URL https://www.sciencedirect.com/science/article/pii/S0021999111004062. Special Issue: Computational Plasma Physics.

[11] Max Duarte, Zdeněk Bonaventura, Marc Massot, and Anne Bourdon. A numerical strategy to discretize and solve the poisson equation on dynamically adapted multiresolution grids for time-dependent streamer discharge simulations. *Journal of Computational Physics*, 289:129–148, 2015. ISSN 0021-9991. doi: https://doi.org/10.1016/j.jcp.2015.02.038. URL https://www.sciencedirect.com/science/article/pii/S0021999115001084.

[12] Zdeněk Bonaventura, Max Duarte, Anne Bourdon, and Marc Massot. Derivation of a merging condition for two interacting streamers in air. *Plasma Sources Science and Technology*, 21(5):052001, aug 2012. doi: 10.1088/0963-0252/21/5/052001. URL https://doi.org/10.1088/0963-0252/21/5/052001.

[13] Z Bonaventura, A Bourdon, S Celestin, and V P Pasko. Electric field determination in streamer discharges in air at atmospheric pressure. *Plasma Sources Science and Technology*, 20(3):035012, apr 2011. doi: 10.1088/0963-0252/20/3/035012. URL https://doi.org/10.1088/0963-0252/20/3/035012.

[14] Adam Obrusník, Petr Bílek, Tomáš Hoder, Milan Šimek, and Zdeněk Bonaventura. Electric field determination in air plasmas from intensity ratio of nitrogen spectral bands: I. Sensitivity analysis and uncertainty quantification of dominant processes. *Plasma Sources Science and Technology*, 27(8):085013, aug 2018. doi: 10.1088/1361-6595/aad663. URL https://doi.org/10.1088/1361-6595/aad663.

[15] Petr Bílek, Adam Obrusník, Tomáš Hoder, Milan Šimek, and Zdeněk Bonaventura. Electric field determination in air plasmas from intensity ratio of nitrogen spectral bands: II. Reduction of the uncertainty and state-of-the-art model. *Plasma Sources Science and Technology*, 27(8):085012, aug 2018. doi: 10.1088/1361-6595/aad666. URL https://doi.org/10.1088/1361-6595/aad666.

[16] Petr Bílek, Milan Šimek, and Zdeněk Bonaventura. Electric field determination from intensity ratio of N_2^+ and N_2 bands: nonequilibrium transient discharges in pure nitrogen. *Plasma Sources Science and Technology*, 28(11):115011, nov 2019. doi: 10.1088/1361-6595/ab3936. URL https://doi.org/10.1088/1361-6595/ab3936.

[17] M Šimek and Z Bonaventura. Non-equilibrium kinetics of the ground and excited states in N_2–O_2 under nanosecond discharge conditions: extended scheme and comparison with available experimental observations. *Journal of Physics D:*

Applied Physics, 51(50):504004, oct 2018. doi: 10.1088/1361-6463/aadcd1. URL https://doi.org/10.1088/1361-6463/aadcd1.

[18] H Raether. Die entwicklung der elektronenlawine in den funkenkanal: Nach beobachtungen in der nebelkammer. *Zeitschrift für Physik*, 112(7-8):464–489, 1939.

[19] Leonard B Loeb and John M Meek. The mechanism of spark discharge in air at atmospheric pressure. i. *Journal of applied physics*, 11(6):438–447, 1940.

[20] JS Townsend. The conductivity produced in gases by the motion of negatively-charged ions. *Nature*, 62(1606):340–341, 1900.

[21] U Ebert, C Montijn, T M P Briels, W Hundsdorfer, B Meulenbroek, A Rocco, and E M van Veldhuizen. The multiscale nature of streamers. *Plasma Sources Science and Technology*, 15(2):S118, apr 2006. doi: 10.1088/0963-0252/15/2/S14. URL https://dx.doi.org/10.1088/0963-0252/15/2/S14.

[22] RV Hodges, RN Varney, and JF Riley. Probability of electrical breakdown: Evidence for a transition between the townsend and streamer breakdown mechanisms. *Physical Review A*, 31(4):2610, 1985.

[23] V P Pasko. Red sprite discharges in the atmosphere at high altitude: the molecular physics and the similarity with laboratory discharges. *Plasma Sources Science and Technology*, 16(1):S13, jan 2007. doi: 10.1088/0963-0252/16/1/S02. URL https://dx.doi.org/10.1088/0963-0252/16/1/S02.

[24] Yuri P Raizer and John E Allen. *Gas discharge physics*, volume 1. Springer, 1991.

[25] Cheng-Ling Kuo, RR Hsu, AB Chen, HT Su, Lou-Chuang Lee, SB Mende, HU Frey, H Fukunishi, and Y Takahashi. Electric fields and electron energies inferred from the isual recorded sprites. *Geophysical research letters*, 32(19), 2005.

[26] SV Pancheshnyi, SV Sobakin, SM Starikovskaya, and A Yu Starikovskii. Discharge dynamics and the production of active particles in a cathode-directed streamer. *Plasma Physics Reports*, 26:1054–1065, 2000.

[27] Yu V Shcherbakov and R S Sigmond. Subnanosecond spectral diagnostics of streamer discharges: Ii. theoretical background. *Journal of Physics D: Applied Physics*, 40(2):474, jan 2007. doi: 10.1088/0022-3727/40/2/024. URL https://dx.doi.org/10.1088/0022-3727/40/2/024.

[28] S M Starikovskaia, K Allegraud, O Guaitella, and A Rousseau. On electric field measurements in surface dielectric barrier discharge. *Journal of Physics D: Applied Physics*, 43(12):124007, mar 2010. doi: 10.1088/0022-3727/43/12/124007. URL https://dx.doi.org/10.1088/0022-3727/43/12/124007.

[29] T Hoder, R Brandenburg, R Basner, K-D Weltmann, K V Kozlov, and H-E Wagner. A comparative study of three different types of barrier discharges in air at atmospheric pressure by cross-correlation spectroscopy. *Journal of Physics D: Applied Physics*, 43(12):124009, mar 2010. doi: 10.1088/0022-3727/43/12/124009. URL https://dx.doi.org/10.1088/0022-3727/43/12/124009.

[30] Tomáš Hoder, R Brandenburg, R Basner, KD Weltmann, KV Kozlov, and HE Wagner. A comparative study of three different types of barrier discharges in air at atmospheric pressure by cross-correlation spectroscopy. *Journal of Physics D: Applied Physics*, 43(12):124009, 2010.

[31] Jingbo Li and Steven Cummer. Estimation of electric charge in sprites from optical and radio observations. *Journal of Geophysical Research: Space Physics*, 116(A1), 2011.

[32] M Šimek. Optical diagnostics of streamer discharges in atmospheric gases. *Journal of Physics D: Applied Physics*, 47(46):463001, 2014.

[33] SA Stepanyan, VR Soloviev, and SM Starikovskaia. An electric field in nanosecond surface dielectric barrier discharge at different polarities of the high voltage pulse: spectroscopy measurements and numerical modeling. *Journal of Physics D: Applied Physics*, 47(48):485201, 2014.

[34] Tomáš Hoder, Mirko Černák, Jean Paillol, Detlef Loffhagen, and Ronny Brandenburg. High-resolution measurements of the electric field at the streamer arrival to the cathode: A unification of the streamer-initiated gas-breakdown mechanism. *Physical Review E*, 86(5):055401, 2012.

[35] Sebastien Celestin and Victor P Pasko. Effects of spatial non-uniformity of streamer discharges on spectroscopic diagnostics of peak electric fields in transient luminous events. *Geophysical Research Letters*, 37(7), 2010.

[36] Alejandro Malagón-Romero, Francisco J Pérez-Invernón, Alejandro Luque, and Francisco J Gordillo-Vázquez. Analysis of the spatial nonuniformity of the electric field in spectroscopic diagnostic methods of atmospheric electricity phenomena. *Journal of Geophysical Research: Atmospheres*, 124(22):12356–12370, 2019.

[37] Sander Nijdam, Jannis Teunissen, and Ute Ebert. The physics of streamer discharge phenomena. *Plasma Sources Science and Technology*, 29(10):103001, 2020.

[38] J Jánský, D Bessiéres, R Brandenburg, J Paillol, and T Hoder. Electric field development in positive and negative streamers on dielectric surface. *Plasma Sources Science and Technology*, 30(10):105008, oct 2021. doi: 10.1088/1361-6595/ac2043. URL `https://dx.doi.org/10.1088/1361-6595/ac2043`.

[39] Benjamin M Goldberg, Tomáš Hoder, and Ronny Brandenburg. Electric field determination in transient plasmas: in situ & non-invasive methods. *Plasma Sources Science and Technology*, 31(7):073001, 2022.

[40] Martina Mrkvičková, Lucia Kuthanová, Petr Bílek, Adam Obrusník, Zdeněk Navrátil, Pavel Dvořák, Igor Adamovich, Milan Šimek, and Tomáš Hoder. Electric field in aptd in nitrogen determined by efish, fns/sps ratio, α-fitting and electrical equivalent circuit model. *Plasma Sources Science and Technology*, 32(6):065009, 2023.

[41] Xiaoran Li, Siebe Dijcks, Anbang Sun, Sander Nijdam, and Jannis Teunissen. Investigation of positive streamers in co2: experiments and 3d particle-in-cell simulations. *Plasma Sources Science and Technology*, 33(9):095009, sep 2024. doi: 10.1088/1361-6595/ad7d35. URL `https://doi.org/10.1088/1361-6595/ad7d35`.

[42] V P Pasko. Blue jets and gigantic jets: transient luminous events between thunderstorm tops and the lower ionosphere. *Plasma Physics and Controlled Fusion*, 50(12):124050, nov 2008. doi: 10.1088/0741-3335/50/12/124050. URL https://dx.doi.org/10.1088/0741-3335/50/12/124050.

[43] Milan Šimek, Martin Člupek, Václav Babický, and Pavel Šunka. Production of reactive species by atmospheric pressure streamers in n2-o2 mixtures. *Pure and Applied Chemistry*, 78(6):1213–1225, 2006. doi: doi:10.1351/pac200678061213. URL https://doi.org/10.1351/pac200678061213.

[44] S M Starikovskaia. Plasma assisted ignition and combustion. *Journal of Physics D: Applied Physics*, 39(16):R265, aug 2006. doi: 10.1088/0022-3727/39/16/R01. URL https://dx.doi.org/10.1088/0022-3727/39/16/R01.

[45] D. D. Sentman, H. C. Stenbaek-Nielsen, M. G. McHarg, and J. S. Morrill. Plasma chemistry of sprite streamers. *Journal of Geophysical Research: Atmospheres*, 113 (D11), 2008. doi: https://doi.org/10.1029/2007JD008941. URL https://agupubs.onlinelibrary.wiley.com/doi/abs/10.1029/2007JD008941.

[46] Alejandro Malagón-Romero, Francisco J. Pérez-Invernón, and Francisco J. Gordillo-Vázquez. Chemical activity of low altitude (50 km) sprite streamers. *Journal of Geophysical Research: Atmospheres*, 128(14):e2023JD038570, 2023. doi: https://doi.org/10.1029/2023JD038570. URL https://agupubs.onlinelibrary.wiley.com/doi/abs/10.1029/2023JD038570. e2023JD038570 2023JD038570.

[47] Baohong Guo and Jannis Teunissen. A computational study on the energy efficiency of species production by single-pulse streamers in air. *Plasma Sources Science and Technology*, 32(2):025001, feb 2023. doi: 10.1088/1361-6595/acb462. URL https://dx.doi.org/10.1088/1361-6595/acb462.

[48] Natalia Yu Babaeva and George V Naidis. Control of plasma jet dynamics by externally applied electric fields. *Plasma Sources Science and Technology*, 30(9): 095003, sep 2021. doi: 10.1088/1361-6595/ac1ee3. URL https://dx.doi.org/10.1088/1361-6595/ac1ee3.

[49] N A Popov. Kinetics of plasma-assisted combustion: effect of non-equilibrium excitation on the ignition and oxidation of combustible mixtures. *Plasma Sources Science and Technology*, 25(4):043002, may 2016. doi: 10.1088/0963-0252/25/4/043002. URL https://dx.doi.org/10.1088/0963-0252/25/4/043002.

[50] Sumire Kobayashi, Zdeněk Bonaventura, Fabien Tholin, Nikolay A Popov, and Anne Bourdon. Study of nanosecond discharges in h2–air mixtures at atmospheric pressure for plasma assisted combustion applications. *Plasma Sources Science and Technology*, 26(7):075004, jun 2017. doi: 10.1088/1361-6595/aa729a. URL https://dx.doi.org/10.1088/1361-6595/aa729a.

[51] K Kourtzanidis, G Dufour, and F Rogier. The electrohydrodynamic force distribution in surface ac dielectric barrier discharge actuators: do streamers dictate the ionic wind profiles? *Journal of Physics D: Applied Physics*, 54(26):26LT01, apr 2021. doi: 10.1088/1361-6463/abf53e. URL https://dx.doi.org/10.1088/1361-6463/abf53e.

[52] I Adamovich, S D Baalrud, A Bogaerts, P J Bruggeman, M Cappelli, V Colombo, U Czarnetzki, U Ebert, J G Eden, P Favia, D B Graves, S Hamaguchi, G Hieftje, M Hori, I D Kaganovich, U Kortshagen, M J Kushner, N J Mason, S Mazouffre, S Mededovic Thagard, H-R Metelmann, A Mizuno, E Moreau, A B Murphy, B A Niemira, G S Oehrlein, Z Lj Petrovic, L C Pitchford, Y-K Pu, S Rauf, O Sakai, S Samukawa, S Starikovskaia, J Tennyson, K Terashima, M M Turner, M C M van de Sanden, and A Vardelle. The 2017 plasma roadmap: Low temperature plasma science and technology. *Journal of Physics D: Applied Physics*, 50(32): 323001, jul 2017. doi: 10.1088/1361-6463/aa76f5. URL `https://dx.doi.org/10.1088/1361-6463/aa76f5`.

[53] I Adamovich, S Agarwal, E Ahedo, L L Alves, S Baalrud, N Babaeva, A Bogaerts, A Bourdon, P J Bruggeman, C Canal, E H Choi, S Coulombe, Z Donkó, D B Graves, S Hamaguchi, D Hegemann, M Hori, H-H Kim, G M W Kroesen, M J Kushner, A Laricchiuta, X Li, T E Magin, S Mededovic Thagard, V Miller, A B Murphy, G S Oehrlein, N Puac, R M Sankaran, S Samukawa, M Shiratani, M Šimek, N Tarasenko, K Terashima, E Thomas Jr, J Trieschmann, S Tsikata, M M Turner, I J van der Walt, M C M van de Sanden, and T von Woedtke. The 2022 plasma roadmap: low temperature plasma science and technology. *Journal of Physics D: Applied Physics*, 55(37):373001, jul 2022. doi: 10.1088/1361-6463/ac5e1c. URL `https://dx.doi.org/10.1088/1361-6463/ac5e1c`.

[54] O. Chanrion and T. Neubert. A pic-mcc code for simulation of streamer propagation in air. *Journal of Computational Physics*, 227(15):7222 – 7245, 2008.

[55] G J M Hagelaar and L C Pitchford. Solving the boltzmann equation to obtain electron transport coefficients and rate coefficients for fluid models. *Plasma Sources Science and Technology*, 14(4):722, 2005. URL `http://stacks.iop.org/0963-0252/14/i=4/a=011`.

[56] S. Pancheshnyi, S. Biagi, M.C. Bordage, G.J.M. Hagelaar, W.L. Morgan, A.V. Phelps, and L.C. Pitchford. The lxcat project: Electron scattering cross sections and swarm parameters for low temperature plasma modeling. *Chemical Physics*, 398:148–153, 2012. ISSN 0301-0104. doi: https://doi.org/10.1016/j.chemphys.2011.04.020. URL `https://www.sciencedirect.com/science/article/pii/S030101041100139X`. Chemical Physics of Low-Temperature Plasmas (in honour of Prof Mario Capitelli).

[57] Leanne C. Pitchford, Luis L. Alves, Klaus Bartschat, Stephen F. Biagi, Marie-Claude Bordage, Igor Bray, Chris E. Brion, Michael J. Brunger, Laurence Campbell, Alise Chachereau, Bhaskar Chaudhury, Loucas G. Christophorou, Emile Carbone, Nikolay A. Dyatko, Christian M. Franck, Dmitry V. Fursa, Reetesh K. Gangwar, Vasco Guerra, Pascal Haefliger, Gerjan J. M. Hagelaar, Andreas Hoesl, Yukikazu Itikawa, Igor V. Kochetov, Robert P. McEachran, W. Lowell Morgan, Anatoly P. Napartovich, Vincent Puech, Mohamed Rabie, Lalita Sharma, Rajesh Srivastava, Allan D. Stauffer, Jonathan Tennyson, Jaime de Urquijo, Jan van Dijk, Larry A. Viehland, Mark C. Zammit, Oleg Zatsarinny, and Sergey Pancheshnyi. Lxcat: an open-access, web-based platform for data needed for modeling low temperature plasmas. *Plasma Processes and Polymers*, 14(1-2):1600098, 2017. doi:

https://doi.org/10.1002/ppap.201600098. URL https://onlinelibrary.wiley.com/doi/abs/10.1002/ppap.201600098.

[58] Emile Carbone, Wouter Graef, Gerjan Hagelaar, Daan Boer, Matthew M. Hopkins, Jacob C. Stephens, Benjamin T. Yee, Sergey Pancheshnyi, Jan van Dijk, and Leanne Pitchford. Data needs for modeling low-temperature non-equilibrium plasmas: The lxcat project, history, perspectives and a tutorial. *Atoms*, 9(1), 2021. ISSN 2218-2004. doi: 10.3390/atoms9010016. URL https://www.mdpi.com/2218-2004/9/1/16.

[59] François Pechereau, Zdeněk Bonaventura, and Anne Bourdon. Influence of surface emission processes on a fast-pulsed dielectric barrier discharge in air at atmospheric pressure. *Plasma Sources Science and Technology*, 25(4):044004, jun 2016. doi: 10.1088/0963-0252/25/4/044004. URL https://dx.doi.org/10.1088/0963-0252/25/4/044004.

[60] Homer D. Hagstrum. Theory of auger ejection of electrons from metals by ions. *Phys. Rev.*, 96:336–365, Oct 1954. doi: 10.1103/PhysRev.96.336. URL https://link.aps.org/doi/10.1103/PhysRev.96.336.

[61] Natalia Yu Babaeva, Cheng Zhang, Jintao Qiu, Xingmin Hou, Victor F Tarasenko, and Tao Shao. The role of fast electrons in diffuse discharge formation: Monte carlo simulation. *Plasma Sources Science and Technology*, 26(8):085008, 2017.

[62] I Odrobina and M Černák. Numerical modeling of the streamer-cathode interaction in a short positive point-plane corona gap. *Czechoslovak journal of physics*, 42(3): 303–315, 1992.

[63] GE Georghiou, R Morrow, and AC Metaxas. The effect of photoemission on the streamer development and propagation in short uniform gaps. *Journal of Physics D: Applied Physics*, 34(2):200, 2001.

[64] Igor Odrobina and Mirko Černák. Numerical simulation of streamer–cathode interaction. *Journal of applied physics*, 78(6):3635–3642, 1995.

[65] Jaroslav Jánský, Fabien Tholin, Zdeněk Bonaventura, and Anne Bourdon. Simulation of the discharge propagation in a capillary tube in air at atmospheric pressure. *Journal of Physics D: Applied Physics*, 43(39):395201, 2010.

[66] Edward Leo Murphy and RH Good Jr. Thermionic emission, field emission, and the transition region. *Physical review*, 102(6):1464, 1956.

[67] R. E. Burgess, H. Kroemer, and J. M. Houston. Corrected values of fowler-nordheim field emission functions $v(y)$ and $s(y)$. *Phys. Rev.*, 90:515–515, May 1953. doi: 10.1103/PhysRev.90.515. URL https://link.aps.org/doi/10.1103/PhysRev.90.515.

[68] Thierry Reess and J Paillol. The role of the field-effect emission in trichel pulse development in air at atmospheric pressure. *Journal of Physics D: Applied Physics*, 30(22):3115, 1997.

[69] J. Paillol, P. Espel, T. Reess, A. Gibert, and P. Domens. Negative corona in air at atmospheric pressure due to a voltage impulse. *Journal of Applied Physics*, 91 (9):5614–5621, 04 2002. ISSN 0021-8979. doi: 10.1063/1.1465124. URL https://doi.org/10.1063/1.1465124.

[70] MB Zheleznyak, AK Mnatsakanyan, and SV Sizykh. Photo-ionization of nitrogen and oxygen mixtures by radiation from a gas discharge. *HIGH TEMPERATURE*, 20(3):357–362, 1982. ISSN 0018-151X.

[71] GW Penney and GT Hummert. Photoionization measurements in air, oxygen, and nitrogen. *Journal of applied physics*, 41(2):572–577, 1970.

[72] Alfred Przybylski. Untersuchung über die 'gasionisierende' strahlung einer entladung. *Zeitschrift für Physik*, 151:264–280, 1958.

[73] Timm H Teich. Emission gasionisierender strahlung aus elektronenlawinen: Ii. messungen in o_2–he-gemischen, dämpfen, co 2 und luft; datenzusammenstellung. *Zeitschrift für Physik*, 199:395–410, 1967.

[74] Timm H Teich. Emission gasionisierender strahlung aus elektronenlawinen: I. messanordnung und messverfahren. messungen in sauerstoff. *Zeitschrift für Physik*, 199:378–394, 1967.

[75] Ningyu Liu and Victor P Pasko. Effects of photoionization on propagation and branching of positive and negative streamers in sprites. *Journal of Geophysical Research: Space Physics*, 109(A4), 2004.

[76] A Kh Mnatsakanyan and GV Naidis. Charged particle production and loss processes in nitrogen-oxygen plasmas. *Reviews of Plasma Chemistry*, 1:259–292, 1991.

[77] A Bourdon, V P Pasko, N Y Liu, S Célestin, P Ségur, and E Marode. Efficient models for photoionization produced by non-thermal gas discharges in air based on radiative transfer and the helmholtz equations. *Plasma Sources Science and Technology*, 16(3):656, aug 2007. doi: 10.1088/0963-0252/16/3/026. URL https://dx.doi.org/10.1088/0963-0252/16/3/026.

[78] Sergey Pancheshnyi. Photoionization produced by low-current discharges in o2, air, n2 and co2. *Plasma Sources Science and Technology*, 24(1):015023, dec 2014. doi: 10.1088/0963-0252/24/1/015023. URL https://dx.doi.org/10.1088/0963-0252/24/1/015023.

[79] R Janalizadeh and VP Pasko. A general framework for photoionization calculations applied to nonthermal gas discharges in air. *Plasma Sources Science and Technology*, 28(10):105006, 2019.

[80] Reza Janalizadeh and Victor P. Pasko. A framework for efficient calculation of photoionization and photodetachment rates with application to the lower ionosphere. *Journal of Geophysical Research: Space Physics*, 125(7):e2020JA027979, 2020. doi: https://doi.org/10.1029/2020JA027979. URL https://agupubs.onlinelibrary.wiley.com/doi/abs/10.1029/2020JA027979. e2020JA027979 10.1029/2020JA027979.

[81] GV Naidis. Modelling of streamer propagation in atmospheric-pressure helium plasma jets. *Journal of Physics D: Applied Physics*, 43(40):402001, 2010.

[82] Amanda M Lietz and Mark J Kushner. Electrode configurations in atmospheric pressure plasma jets: production of reactive species. *Plasma Sources Science and Technology*, 27(10):105020, oct 2018. doi: 10.1088/1361-6595/aadf5b. URL https://dx.doi.org/10.1088/1361-6595/aadf5b.

[83] Anne Bourdon, Thibault Darny, François Pechereau, Jean-Michel Pouvesle, Pedro Viegas, Sylvain Iséni, and Eric Robert. Numerical and experimental study of the dynamics of a μs helium plasma gun discharge with various amounts of n2 admixture. *Plasma Sources Science and Technology*, 25(3):035002, mar 2016. doi: 10.1088/0963-0252/25/3/035002. URL https://dx.doi.org/10.1088/0963-0252/25/3/035002.

[84] Reza Janalizadeh and Victor P Pasko. Photoionization of air species as impurities in atmospheric pressure helium plasma. *Plasma Sources Science and Technology*, 32(9):095011, sep 2023. doi: 10.1088/1361-6595/acf7e8. URL https://doi.org/10.1088/1361-6595/acf7e8.

[85] Natalia Yu Babaeva, Cheng Zhang, Jintao Qiu, Xingmin Hou, Victor F Tarasenko, and Tao Shao. The role of fast electrons in diffuse discharge formation: Monte carlo simulation. *Plasma Sources Science and Technology*, 26(8):085008, aug 2017. doi: 10.1088/1361-6595/aa7bb0. URL https://doi.org/10.1088/1361-6595/aa7bb0.

[86] J Stephens, M Abide, A Fierro, and A Neuber. Practical considerations for modeling streamer discharges in air with radiation transport. *Plasma Sources Science and Technology*, 27(7):075007, 2018.

[87] Robert Marskar. 3d fluid modeling of positive streamer discharges in air with stochastic photoionization. *Plasma Sources Science and Technology*, 29(5):055007, may 2020. doi: 10.1088/1361-6595/ab87b6. URL https://dx.doi.org/10.1088/1361-6595/ab87b6.

[88] B Bagheri and J Teunissen. The effect of the stochasticity of photoionization on 3d streamer simulations. *Plasma Sources Science and Technology*, 28(4):045013, apr 2019. doi: 10.1088/1361-6595/ab1331. URL https://dx.doi.org/10.1088/1361-6595/ab1331.

[89] Andrew Fierro, Chris Moore, Ben Yee, and Matthew Hopkins. Three-dimensional kinetic modeling of streamer propagation in a nitrogen/helium gas mixture. *Plasma Sources Science and Technology*, 27(10):105008, oct 2018. doi: 10.1088/1361-6595/aae055. URL https://dx.doi.org/10.1088/1361-6595/aae055.

[90] P Ségur, A Bourdon, E Marode, D Bessieres, and J H Paillol. The use of an improved eddington approximation to facilitate the calculation of photoionization in streamer discharges. *Plasma Sources Science and Technology*, 15(4):648–660, July 2006. doi: 10.1088/0963-0252/15/4/009. URL https://doi.org/10.1088/0963-0252/15/4/009.

[91] Alejandro Luque, Ute Ebert, Carolynne Montijn, and Willem Hundsdorfer. Photoionization in negative streamers: Fast computations and two propagation modes. *Applied Physics Letters*, 90(8):081501, February 2007. doi: 10.1063/1.2435934. URL https://doi.org/10.1063/1.2435934.

[92] S Chandrasekhar. *Radiative Transfer*. Dover Books on Physics. Dover Publications, Mineola, NY, March 2003.

[93] Michael F. Modest. *Radiative Heat Transfer, Third Edition*. Elsevier Science;Academic Press, 3ed. edition, 2013. ISBN 9780123869449.

[94] Edward W. Larsen, Guido Thömmes, Axel Klar, Mohammed Seaid, and Thomas Götz. Simplified PN approximations to the equations of radiative heat transfer and applications. *Journal of Computational Physics*, 183(2):652–675, December 2002. doi: 10.1006/jcph.2002.7210. URL https://doi.org/10.1006/jcph.2002.7210.

[95] K. D. Lathrop. Use of discrete-ordinates methods for solution of photon transport problems. *Nuclear Science and Engineering*, 24(4):381–388, April 1966. doi: 10.13182/nse66-a16408. URL https://doi.org/10.13182/nse66-a16408.

[96] W. A. Fiveland. Discrete-ordinates solutions of the radiative transport equation for rectangular enclosures. *Journal of Heat Transfer*, 106(4):699–706, November 1984. doi: 10.1115/1.3246741. URL https://doi.org/10.1115/1.3246741.

[97] S.A. Clough, M.W. Shephard, E.J. Mlawer, J.S. Delamere, M.J. Iacono, K. Cady-Pereira, S. Boukabara, and P.D. Brown. Atmospheric radiative transfer modeling: a summary of the AER codes. *Journal of Quantitative Spectroscopy and Radiative Transfer*, 91(2):233–244, March 2005. doi: 10.1016/j.jqsrt.2004.05.058. URL https://doi.org/10.1016/j.jqsrt.2004.05.058.

[98] K. Sumiyoshi and S. Yamada. NEUTRINO TRANSFER IN THREE DIMENSIONS FOR CORE-COLLAPSE SUPERNOVAE. i. STATIC CONFIGURATIONS. *The Astrophysical Journal Supplement Series*, 199(1):17, February 2012. doi: 10.1088/0067-0049/199/1/17. URL https://doi.org/10.1088/0067-0049/199/1/17.

[99] C Lee. THE DISCRETE sn APPROXIMATION TO TRANSPORT THEORY. Technical report, Los Alamos Scientific Laboratory, June 1961. URL https://doi.org/10.2172/4783088.

[100] G. D. Raithby and E. H. Chui. A finite-volume method for predicting a radiant heat transfer in enclosures with participating media. *Journal of Heat Transfer*, 112(2):415–423, May 1990. doi: 10.1115/1.2910394. URL https://doi.org/10.1115/1.2910394.

[101] J. Murthy and S. Mathur. A finite volume method for radiative heat transfer using unstructured meshes. In *36th AIAA Aerospace Sciences Meeting and Exhibit*. American Institute of Aeronautics and Astronautics, January 1998. doi: 10.2514/6.1998-860. URL https://doi.org/10.2514/6.1998-860.

[102] S. R. Mathur and J. Y. Murthy. Coupled ordinates method for multigrid acceleration of radiation calculations. *Journal of Thermophysics and Heat Transfer*, 13(4): 467–473, October 1999. doi: 10.2514/2.6485. URL https://doi.org/10.2514/2.6485.

[103] G V Naidis. On photoionization produced by discharges in air. *Plasma Sources Science and Technology*, 15(2):253–255, March 2006. doi: 10.1088/0963-0252/15/2/010. URL https://doi.org/10.1088/0963-0252/15/2/010.

[104] Carolynne Montijn, Willem Hundsdorfer, and Ute Ebert. An adaptive grid refinement strategy for the simulation of negative streamers. *Journal of Computational Physics*, 219(2):801–835, 2006.

[105] GJM Hagelaar and GMW Kroesen. Speeding up fluid models for gas discharges by implicit treatment of the electron energy source term. *Journal of Computational Physics*, 159(1):1–12, 2000.

[106] Max Duarte, Marc Massot, Stéphane Descombes, Christian Tenaud, Thierry Dumont, Violaine Louvet, and Frédérique Laurent. New resolution strategy for multiscale reaction waves using time operator splitting, space adaptive multiresolution, and dedicated high order implicit/explicit time integrators. *SIAM Journal on Scientific Computing*, 34(1):A76–A104, 2012.

[107] Ami Harten. Multiresolution algorithms for the numerical solution of hyperbolic conservation laws. *Communications on Pure and Applied Mathematics*, 48(12): 1305–1342, 1995. doi: https://doi.org/10.1002/cpa.3160481201. URL https://onlinelibrary.wiley.com/doi/abs/10.1002/cpa.3160481201.

[108] Albert Cohen, Sidi Kaber, Siegfried Müller, and Marie Postel. Fully adaptive multiresolution finite volume schemes for conservation laws. *Mathematics of computation*, 72(241):183–225, 2003.

[109] C T R Wilson. The electric field of a thundercloud and some of its effects. *Proceedings of the Physical Society of London*, 37(1):32D, jan 1924. doi: 10.1088/1478-7814/37/1/314. URL https://doi.org/10.1088/1478-7814/37/1/314.

[110] R. C. Franz, R. J. Nemzek, and J. R. Winckler. Television image of a large upward electrical discharge above a thunderstorm system. *Science*, 249(4964):48–51, 1990. doi: 10.1126/science.249.4964.48. URL https://www.science.org/doi/abs/10.1126/science.249.4964.48.

[111] Joseph R Dwyer, David M Smith, and Steven A Cummer. High-energy atmospheric physics: Terrestrial gamma-ray flashes and related phenomena. *Space Science Reviews*, 173(1):133–196, 2012.

[112] A.V. Gurevich, G.M. Milikh, and R. Roussel-Dupre. Runaway electron mechanism of air breakdown and preconditioning during a thunderstorm. *Physics Letters A*, 165(5):463–468, 1992. ISSN 0375-9601. doi: https://doi.org/10.1016/0375-9601(92)90348-P. URL https://www.sciencedirect.com/science/article/pii/037596019290348P.

[113] J. R. Dwyer. A fundamental limit on electric fields in air. *Geophysical Research Letters*, 30(20), 2003. doi: https://doi.org/10.1029/2003GL017781. URL https://agupubs.onlinelibrary.wiley.com/doi/abs/10.1029/2003GL017781.

[114] G. J. Fishman, P. N. Bhat, R. Mallozzi, J. M. Horack, T. Koshut, C. Kouveliotou, G. N. Pendleton, C. A. Meegan, R. B. Wilson, W. S. Paciesas, S. J. Goodman, and H. J. Christian. Discovery of intense gamma-ray flashes of atmospheric origin. *Science*, 264(5163):1313–1316, 1994. doi: 10.1126/science.264.5163.1313. URL https://www.science.org/doi/abs/10.1126/science.264.5163.1313.

[115] N. G. Lehtinen, T. F. Bell, and U. S. Inan. Monte carlo simulation of runaway mev electron breakdown with application to red sprites and terrestrial gamma ray flashes. *Journal of Geophysical Research: Space Physics*, 104(A11): 24699–24712, 1999. doi: https://doi.org/10.1029/1999JA900335. URL https://agupubs.onlinelibrary.wiley.com/doi/abs/10.1029/1999JA900335.

[116] Sebastien Celestin and Victor P Pasko. Soft collisions in relativistic runaway electron avalanches. *Journal of Physics D: Applied Physics*, 43(31):315206, jul 2010. doi: 10.1088/0022-3727/43/31/315206. URL https://doi.org/10.1088/0022-3727/43/31/315206.

[117] Francoise Massines, Christian Sarra-Bournet, Fiorenza Fanelli, Nicolas Naudé, and Nicolas Gherardi. Atmospheric Pressure Low Temperature Direct Plasma Technology: Status and Challenges for Thin Film Deposition. *Plasma Processes and Polymers*, 9(11-12):1041–1073, 2012. doi: https://doi.org/10.1002/ppap.201200029. URL https://onlinelibrary.wiley.com/doi/abs/10.1002/ppap.201200029.

[118] Sergey B Leonov, Igor V Adamovich, and Victor R Soloviev. Dynamics of near-surface electric discharges and mechanisms of their interaction with the airflow. *Plasma Sources Science and Technology*, 25(6):063001, nov 2016. doi: 10.1088/0963-0252/25/6/063001. URL https://dx.doi.org/10.1088/0963-0252/25/6/063001.

[119] S M Starikovskaia. Plasma-assisted ignition and combustion: nanosecond discharges and development of kinetic mechanisms. *Journal of Physics D: Applied Physics*, 47(35):353001, aug 2014. doi: 10.1088/0022-3727/47/35/353001. URL https://dx.doi.org/10.1088/0022-3727/47/35/353001.

[120] U. Czarnetzki, D. Luggenhölscher, and H. F. Döbele. Sensitive Electric Field Measurement by Fluorescence-Dip Spectroscopy of Rydberg States of Atomic Hydrogen. *Phys. Rev. Lett.*, 81:4592–4595, Nov 1998. doi: 10.1103/PhysRevLett.81.4592. URL https://link.aps.org/doi/10.1103/PhysRevLett.81.4592.

[121] Arthur Dogariu, Benjamin M. Goldberg, Sean O'Byrne, and Richard B. Miles. Species-Independent Femtosecond Localized Electric Field Measurement. *Phys. Rev. Appl.*, 7:024024, Feb 2017. doi: 10.1103/PhysRevApplied.7.024024. URL https://link.aps.org/doi/10.1103/PhysRevApplied.7.024024.

[122] Benjamin M Goldberg, Tomáš Hoder, and Ronny Brandenburg. Electric field determination in transient plasmas: in situ & non-invasive methods. *Plasma Sources Science and Technology*, 31(7):073001, sep 2022. doi: 10.1088/1361-6595/ac6e03. URL https://dx.doi.org/10.1088/1361-6595/ac6e03.

[123] Goran B Sretenović, Ivan B Krstić, Vesna V Kovačević, Bratislav M Obradović, and Milorad M Kuraica. Spatio-temporally resolved electric field measurements in helium plasma jet. *Journal of Physics D: Applied Physics*, 47(10):102001, feb 2014. doi: 10.1088/0022-3727/47/10/102001. URL https://dx.doi.org/10.1088/0022-3727/47/10/102001.

[124] Vesna V Kovačević, Goran B Sretenović, Elmar Slikboer, Olivier Guaitella, Ana Sobota, and Milorad M Kuraica. The effect of liquid target on a nonthermal plasma jet—imaging, electric fields, visualization of gas flow and optical emission spectroscopy. *Journal of Physics D: Applied Physics*, 51(6):065202, jan 2018. doi: 10.1088/1361-6463/aaa288. URL https://dx.doi.org/10.1088/1361-6463/aaa288.

[125] K V Kozlov, H-E Wagner, R Brandenburg, and P Michel. Spatio-temporally resolved spectroscopic diagnostics of the barrier discharge in air at atmospheric pressure. *Journal of Physics D: Applied Physics*, 34(21):3164, oct 2001. doi: 10.1088/0022-3727/34/21/309. URL https://dx.doi.org/10.1088/0022-3727/34/21/309.

[126] Saša S Ivković, Goran B Sretenović, Bratislav M Obradović, Nikola Cvetanović, and Milorad M Kuraica. On the use of the intensity ratio of He lines for electric field measurements in atmospheric pressure dielectric barrier discharge. *Journal of Physics D: Applied Physics*, 47(5):055204, jan 2014. doi: 10.1088/0022-3727/47/5/055204. URL https://dx.doi.org/10.1088/0022-3727/47/5/055204.

[127] P Paris, M Aints, M Laan, and F Valk. Measurement of intensity ratio of nitrogen bands as a function of field strength. *Journal of Physics D: Applied Physics*, 37(8):1179, mar 2004. doi: 10.1088/0022-3727/37/8/005. URL https://doi.org/10.1088/0022-3727/37/8/005.

[128] P Paris, M Aints, F Valk, T Plank, A Haljaste, K V Kozlov, and H-E Wagner. Intensity ratio of spectral bands of nitrogen as a measure of electric field strength in plasmas. *Journal of Physics D: Applied Physics*, 38(21):3894, oct 2005. doi: 10.1088/0022-3727/38/21/010. URL https://doi.org/10.1088/0022-3727/38/21/010.

[129] YLM Creyghton. Pulsed positive corona discharges: fundamental study and application to flue gas treatment. *Eidhoven University of Technology*, 1994.

[130] S Pancheshnyi. Comments on 'intensity ratio of spectral bands of nitrogen as a measure of electric field strength in plasmas'. *Journal of Physics D: Applied Physics*, 39(8):1708, mar 2006. doi: 10.1088/0022-3727/39/8/N01. URL https://doi.org/10.1088/0022-3727/39/8/N01.

[131] Mario Capitelli, Carlos M Ferreira, Boris F Gordiets, and Alexey I Osipov. *Plasma kinetics in atmospheric gases*, volume 31. Springer Science & Business Media, 2013.

[132] I A Kossyi, A Yu Kostinsky, A A Matveyev, and V P Silakov. Kinetic scheme of the non-equilibrium discharge in nitrogen-oxygen mixtures. *Plasma Sources Science and Technology*, 1(3):207, aug 1992. doi: 10.1088/0963-0252/1/3/011. URL https://doi.org/10.1088/0963-0252/1/3/011.

[133] B.F. Gordiets, C.M. Ferreira, V.L. Guerra, J.M.A.H. Loureiro, J. Nahorny, D. Pagnon, M. Touzeau, and M. Vialle. Kinetic model of a low-pressure N_2-O_2 flowing glow discharge. *IEEE Transactions on Plasma Science*, 23(4):750–768, 1995. doi: 10.1109/27.467998.

[134] A Flitti and S Pancheshnyi. Gas heating in fast pulsed discharges in N2–O2 mixtures. *The European Physical Journal Applied Physics*, 45(2):21001, 2009.

[135] Max D. Morris. Factorial sampling plans for preliminary computational experiments. *Technometrics*, 33(2):161–174, 1991. doi: 10.1080/00401706.1991.10484804.

[136] AF Djakov, Yu K Bobrov, LN Bobrova, and Yu V Yourguelenas. Streamer discharge plasma parameters determination in air on a base of a measurement of radiation of the molecular bands of nitrogen. *Physics and Technology of Electric Power Transmission*, 1:219–233, 1998.

[137] Yongho Kim, Sang Hee Hong, Min Suk Cha, Young-Hoon Song, and Seock Joon Kim. Measurements of electron energy by emission spectroscopy in pulsed corona and dielectric barrier discharges. *Journal of Advanced Oxidation Technologies*, 6(1): 17–22, 2003. doi: doi:10.1515/jaots-2003-0103. URL `https://doi.org/10.1515/jaots-2003-0103`.

[138] T Hoder, P Synek, D Chorvát, J Ráhel', R Brandenburg, and M Černák. Complex interaction of subsequent surface streamers via deposited charge: a high-resolution experimental study. *Plasma Physics and Controlled Fusion*, 59(7): 074001, may 2017. doi: 10.1088/1361-6587/aa6ea2. URL `https://doi.org/10.1088/1361-6587/aa6ea2`.